

1 **Conjugated polymer for implantable electronics towards clinical**
2 **application**

3
4 Yuxin Liu¹, Vivian Rachel Feig², Zhenan Bao³

5
6 ¹ Institute of Materials Research and Engineering, Agency for Science, Technology and Research,
7 Singapore

8 ²Division of Gastroenterology, Brigham and Women's Hospital, Harvard Medical School, Boston,
9 MA, USA

10 ³Department of Chemical Engineering, Stanford University, Stanford, CA, USA.

11
12 **Abstract**

13 Owing to their excellent mechanical flexibility, mixed-conducting electrical property, and
14 extraordinary chemical tunability, conjugated polymers have been demonstrated to be an ideal
15 bioelectronic interface to deliver therapeutic effect in many different chronic diseases. This
16 review article summarizes the latest advances in implantable electronics using conjugated
17 polymers as electroactive materials and identifies remaining challenges and opportunities for
18 developing electronic medicine. We selectively reviewed examples of conjugated polymer-based
19 bioelectronic devices in human clinical studies or animal studies with the potential for clinical
20 adoption. The unique properties of conjugated polymers are highlighted and exemplified as
21 potential solutions to address the specific challenges in electronic medicine.

22
23 **Introduction**

24 Electronic medicine is an emerging field that uses electricity to regulate and interact with
25 biological tissues, especially electrogenic tissue, delivering high-temporospatial-resolution and
26 personalized therapy. In the past two decades, the rapid development of organic bioelectronics
27 and understanding of neurophysiology (e.g. inflammatory reflex) opens up many opportunities.
28 Electronic medicine have been used to treat a variety of chronic diseases, such as atrial
29 fibrillation, epilepsy and Parkinson's disease by sending or collecting electrical signals. In
30 contrast to pharmaceutical medicine that modulates biochemical signaling in biological systems,
31 electronic medicine transports charges across the interface between electronics and biological
32 tissue to manage and treat diseases. Implantable electronic medicine has been used to treat
33 millions of patients, with an expected annual market size of over 20 billion by 2022¹. For drug-
34 resistant diseases, such as drug-resistant epilepsy, electronic medicine serves as the last resort
35 for alleviating the symptoms.

36
37 In current clinical practice, metal-based conductors, such as platinum and gold, remain the
38 primary electronic materials to inject charges in and out of the biotic-abiotic interface. However,
39 conjugated polymers, with their unique mechanical, chemical, and electrical properties, are
40 becoming an attractive alternative for interfacing with biological tissue. Common conjugated
41 polymers with biomedical potential include semiconducting polymer²⁻⁹ such as poly(3-
42 hexylthiophene) (P3HT)¹⁰ and conducting polymer such as poly(3,4-ethylenedioxythiophene)
43 polystyrene sulfonate (PEDOT:PSS)¹¹, polyaniline¹², polypyrrole(Ppy)¹³ (**Figure 1**).

44
45 In this review, we summarize the latest advances on using conjugated polymers for implantable
46 electronics. We do not include on-skin wearable electronics, which have been extensively

48 covered by other reviews¹⁴⁻¹⁶. We focus specifically on polymeric devices that have been shown
49 feasibilities in human clinical studies or animal studies with potential for clinical adoption. In the
50 clinical applications, conjugated polymers play a critical role for delivering charges to modulate
51 electrogenic tissues, and for sensing the electrophysiological signals and controlling the release
52 of biomolecular compounds at the interfaced tissues. The review is structured according to
53 different biological and clinical applications that exemplify and highlight one or more unique
54 properties of conducting polymers. In the following sections, we will first highlight some of the
55 unique advantages of conjugated polymers in bioelectronics. The following sections are
56 organized based on clinically-relevant and disease-associated physiological application including
57 intracranial, peripheral nerve, cardiac, biomolecular, and emerging distributed interfaces. The
58 review concludes with pointing out the remaining challenges and opportunities for developing
59 clinically-translatable conjugated polymer-based tissue-mimicking implantable electronics.

60

61

62 1. Advantages of conjugated polymers in bioelectronics

63

64 **Mixed conductor** Electrophysiological communication and function of biological tissues and cells
65 is based on the mobility of the hydrated ions presented in intra- and extracellular environment.
66 The mismatch of the ionic conduction in electrogenic tissues and electronic conduction in
67 conventional inorganic materials pose a challenge for effective electrical therapeutics. Different
68 from metal conductors, conjugated polymers form contiguous SP^2 -hybridized carbon centers
69 with alternating double and single bonds in the backbone. The delocalized π -orbitals facilitate
70 charge transport intra- and intermolecularly¹⁷. Doping is a common strategy to increase the
71 conductivity of conjugated polymers by charge transfer to or from the doping molecules to the
72 conjugated polymer to generate mobile charge carriers. Besides electronic conductance, doped
73 conjugated polymers also mediate ionic conductance when interfaced with wet biological
74 tissues due to the presence of ionic moieties. The three-dimensional micro/nanoporous polymer
75 structure increases the surface area for electrostatic double-layer capacitive effect, resulting in
76 volumetric contribution to the impedance at the interface, compared with a non-porous and
77 pure metallic electrode (e.g. gold electrode). The ionic conductance originates from mobile ions
78 (e.g. sodium, potassium ions or proton) transporting through the ionic medium containing ionic
79 dopants (e.g. polystyrene sulfonate) and doped conjugated polymers (positive or negatively
80 charged depending on whether p-doping or n-doping)¹⁸. The mixed (both ionic and electronic)
81 conductivity characteristic of conjugated polymers make them an ideal interface between ionic-
82 mediated biological systems and electronic-mediated device circuits, offering reduced
83 electrochemical impedance, higher current density, and higher signal-to-noise ratio¹⁹⁻²¹.

84

85 **Chemical tunability** There is abundant design space to chemically modify the side chains or
86 conjugated polymer backbones to better mimic properties of biological systems. Self-healing²²⁻
87 ²⁴, degradable^{25,26}, and biologically-responsive²⁷ properties can be introduced to conjugated
88 polymers. Cell adhesion can be improved by various chemical and electrochemical methods,
89 including functionalization of hydrophilic groups²⁸ (e.g. amine group) or arginylglycylaspartic
90 acid (RGD) peptide²⁹ on conducting polymer side chain, selecting appropriate dopant (e.g.
91 poly(2-methoxyaniline-5-sulfonicacid) (PMAS) and chondroitin sulphate (CS)³⁰) and electrically
92 switching conjugated polymer to partially reduced states³¹. In addition, the polymeric matrix can
93 be chemically engineered to host biomolecules and drugs. For example, pharmaceutical drugs
94 can serve as dopants in oxidized conjugated polymers and subsequently be released with
95 electrical^{32,33}.

96
97 **Biomechanical compatibility** Localized (bidirectional) signal communication with high
98 temporospatial resolution requires a soft and stretchable electronic interface, because
99 interfaced biological tissues are viscoelastic, curvy, constantly moving and dynamic. Conjugated
100 polymers with these properties have been designed to accommodate these unique features of
101 biological tissue. By engineering Young's modulus, intrinsic stretchability, and other mechanical
102 properties of conjugated polymers (Young's modulus \sim 100s MPa-GPa) and especially electrically
103 conductive hydrogels (Young's modulus \sim kPa), the large mechanical mismatch that exists
104 between conventional rigid electronics (Young's modulus \sim GPa - TPa) and biological tissue
105 (Young's modulus \sim kPa) can be closed^{34,35}. As a result, the biomechanical compatible bio-
106 interface preserves the biomechanical microenvironment and can reduce or even eliminate
107 immunoresponse and scar tissue formation, which are common problems in current clinically
108 implanted electronics³⁶⁻³⁸.

109
110
111 **2. Intracranial neural interface**

112 Different from scalp-recorded electroencephalography (EEG), intracranial electrodes direct
113 interface with brain tissue underneath the skull. As one of the most commonly used neural
114 interfaces for both clinical and research purposes, intracranial electrodes show promise in
115 regaining motor function³⁹, memory⁴⁰, sensory function⁴¹ and recently, speech ability⁴². In
116 clinical practice, epilepsy, especially drug-resistant epilepsy (accounting for one-third of total
117 epilepsy cases⁴³) requires implantation of intracranial electrode arrays for electrophysiological
118 recording and stimulation. Electrophysiological recording with intracranial electrode arrays
119 identifies the epileptic zone for subsequent removal; at the same time, microstimulation
120 functionally maps out the eloquent cortical region to avoid surgical damage. Intracranial
121 electrode arrays take different form factors for electrocorticography (ECoG) and stereotaxic EEG
122 (sEEG). ECoG electrode grids are thin membranes with a two-dimensional surface that are
123 implanted on the brain surface in the subdural region (e.g. for epilepsy), while sEEG electrodes
124 are often thin wires that are inserted deep into the brain, in order to record or stimulate deeper
125 brain tissues (e.g. for Parkinson's disease).⁴⁴

126
127 **Accommodating irregular shape and curvilinear cerebral cortex**

128 The human cerebral cortex undergoes gyration and forms ridges (i.e. gyrus) and depressions
129 (sulcus). Each gyrus has a size⁴⁴ of \sim 6 cm². The highly irregular and curvilinear surface creates
130 difficulty for conventional rigid electronics and requires a flexible electrode array to form an
131 intimate interface. Typical thin plastic substrates (tens of micron meters) such as polyimide and
132 evaporated metal interconnects allow relatively low bending radii and can, only to a certain
133 degree (Intrasulcal space remains a challenge to access without delicate microdissection due to
134 its deep structure⁴⁵), conform with the gyrus for ECoG and microelectrocorticography (μ ECoG).
135 The conducting polymer PEDOT:PSS can be readily electropolymerized on the metal (e.g. gold)
136 to form a flexible thin-film form factor for direct electrochemical interfacing to the brain
137 cortex^{46,47}. The thickness of encapsulated devices, including conducting polymer and insulation
138 layers, can be reduced to around 10 μ m to decrease the bending stiffness, which is proportional
139 to the inverse cube of thickness.^{46,48} Lee et al. developed a ultraflexible ECoG electrode array
140 with thickness of only 2.6 μ m. The electrode array were arranged in a honeycomb mesh to allow
141 structural stretchability⁴⁹. Besides structural (e.g. shape and dimension) engineering,
142 researchers have developed bioelectronics with soft polymeric materials as an alternative
143 approach to conform with curvilinear surface of the brain. Blau et al. fabricated an all-polymer

144 multielectrode array with PEDOT:PSS and graphite- polydimethylsiloxane (PDMS) as
145 conductor.⁵⁰ The soft electrode array successfully recorded local field potential (LFP) responses
146 to patterned visual stimuli *in vivo* on primary visual cortex of rats.

147

148 **Shrinking electrode area requires lower impedance**

149 Missing important epileptic areas during EcoG mapping happens due to low electrode density,
150 which gives relatively large interelectrode space . As a result, seizures cannot be eradicated in
151 many epilepsy surgeries⁵¹. A large electrode area also diminishes the heterogeneity of local
152 neural activity and leads to attenuation of high-frequency signals, such as high-gamma signals
153 (originated from non-oscillatory synaptic activity) and abnormal high-frequency oscillations
154 (HFOs), which are important for identification of seizure foci⁵².

155

156 Reducing the electrode size and increasing the electrode density (the number of electrodes per
157 unit area) will allow more localized identification of neural activity (e.g. HFOs) for physicians,
158 but, at the same time, pose the challenge of higher electrochemical impedance, because the
159 impedance of non-porous electrode materials (e.g. platinum) is inversely proportional to the
160 geometrical size. Unlike electrophysiological recordings in research labs, where electrical noise is
161 well-controlled (e.g. with use of Faraday cages), ECoG recording in surgical rooms suffer from
162 extensive electromagnetic noise from other essential medical equipment and therefore requires
163 especially low electrochemical impedance. For a conventional (clinically-used) electrode with a
164 size of ~2 mm and an inter-electrode spacing of 1 cm, the impedance can be kept below kilo-
165 ohm levels. With the same metal-based electronic materials, the impedance (at 1000 Hz) goes
166 up to mega-ohm levels if one reduces the electrode size to be comparable to the size of a single
167 neuron (~20 μ m).

168

169 Coating the metal electrode with additional layers of conducting polymer is an effective way to
170 decrease impedance. Abidian et al. reported that the impedance of the electrode reduced by
171 two orders of magnitude at the electrophysiological-relevant frequency of 1000 Hz after
172 modification with poly(3,4-ethylenedioxythiophene) (PEDOT)-based materials⁵³. To further
173 reduce the electrode size, Khodagholy and co-workers demonstrated NeuroGrid⁵⁴ that recorded
174 EcoG signal with an electrode size of 10 μ m (**Figure 2A**). The free-standing PEDOT:PSS
175 microelectrodes were lithographically patterned using paralyene as a sacrificial layer⁵⁵. The
176 impedance of NeuroGrid electrodes (~2 \times 10⁴ Ohm) was more than ten times lower than that of
177 gold electrodes or silicon probes. Because the electrode size matched that of neuronal bodies, it
178 was shown to record both local field potentials and putative single-unit action potentials
179 without the need for brain penetration in two human patients during epilepsy surgery (**Figure**
180 **2B**). In a separate study⁵⁶, PEDOT:PSS electrodes (**Figure 2C**) with slightly larger areas (e.g. 50
181 μ m in diameter) were unable to record action potentials, highlighting the importance of using
182 high-density and high spatial resolution electrode arrays. Nevertheless, the conducting polymer-
183 coated electrode was capable of recording stimulus-locked cognitive activity within a distance of
184 400 μ m. Besides, the device recorded a noticeable increase in epileptiform activity 200s after
185 administration of Methohexitol, a drug that is known to induce seizures (**Figure 2D**). The
186 PEDOT:PSS maintained its mechanical and electrochemical performance after autoclave
187 sterilization, an essential step for clinical application. Recently, a clinical study (**Figure 2E**)
188 involving 30 human participants demonstrated reliable intracranial monitoring by PEDOT:PSS
189 microelectrodes during surgical resection⁵⁷. The low impedance electrode could record unitary
190 events that can be specifically modulated by different external stimuli.

191

192 How do conducting polymers like PEDOT:PSS substantially reduce electrochemical impedance to
193 form a low impedance interface with ionically-conductive tissue? **Many doped conjugated**
194 **polymers exhibit mixed conductor properties. That means the conducting polymer electrode can**
195 **be modeled as having both a capacitor and a resistor in parallel. At lower frequency, the**
196 **capacitive contribution, especially from the porous nature of the conducting polymer can help**
197 **to significantly reduce the overall impedance at the interface (Figure 2F). This makes them ideal**
198 **for direct interfacing with biological systems^{58,59}.**

199

200 ***Exploiting high transconductance of conjugated polymer based electrochemical transistor***

201 The drain current in organic electrochemical transistors (OECT) can be controlled by the
202 injection of ions into conjugated polymers, owing to their mixed conduction and high ionic
203 mobility¹⁸. Khodagholy et al. reported that OECTs had superior signal-to-noise ratio compared to
204 conventional surface electrodes⁶⁰ (Figure 3A). PEDOT:PSS was used as semiconducting channel,
205 and a noble metal was used as the source and drain. The high transconductance (900 μ S) of the
206 PEDOT-based OECT⁶¹ amplified the small potential on the brain surface (in the range of μ V). The
207 PEDOT-based OECT demonstrated superior signal-to-noise ratio for recording of surface low-
208 amplitude brain activities, which were poorly resolved with surface electrodes (Figure 3B).

209

210 ECoG mapping of drug-induced epilepsy *in vivo* showed local field potential (summation of a
211 group of neural activity), but single-unit-like electrophysiological signals were not observed,
212 although the electrode size used was comparable to that of Neurogrid. One possible reason can
213 be that the response speed of traditional OECTs is not fast enough to accommodate millisecond-
214 scale action potentials⁶². In such cases, one can only back-calculate the voltage by using
215 complicated modeling with known device parameters, which is impractical in clinical
216 applications. More recently, the enhancement-mode, internal ion-gated organic electrochemical
217 transistor (e-IGT) developed by Cea et al. demonstrated high operational speed with a short rise
218 time of 2.9 μ s while maintaining \sim 1.5mS transconductance⁶³ (Figure 3C). When the device is in
219 the “off” state, the amine group on polyethylenimine (PEI) transfers electrons to PEDOT:PSS,
220 forming PEDOT⁰. Once the gate voltage becomes negative, PEI⁺ is compensated and PSS⁻ re-
221 dopes the PEDOT, leading to a dramatic increase of channel conduction. Action potentials were
222 successfully recorded in freely moving epileptic rats with improved response time. Compared
223 with microelectrodes, the key advantage of using an electrochemical transistor is that it can
224 locally amplify the signal, which improves the signal quality, especially when long interconnects
225 are used or an electrically noisy environment is present (Figure 3D). In addition, an active OECT
226 matrix can minimize the number of interconnecting wires by the factor of M+N-NxM, where N
227 and M are the number of rows and columns, respectively⁶⁴. This is important to reduce the
228 number of interconnects needed for large-scale high-density electrophysiological mapping. As a
229 powerful alternative to microelectrodes, it has the potential to be tested and deployed for
230 intraoperative ECoG in hospitals in the near future.

231

232 ***Conjugated polymer-based penetrating electrodes with reduced immunoresponse***

233

234 Penetrating electrodes are needed to access epileptic regions hidden in the deep cerebral cortex
235 and for deep brain stimulation to treat neurological disorders. Compared with ECoG electrodes,
236 penetrating electrodes are advantageous for capturing single-unit neural activity due to the
237 proximity of the electrode to individual neurons. At the same time, penetrating electrodes are
238 more invasive and pose a higher risk for adverse immunoresponse, especially for nervous
239 tissues. After neuroelectronic implantation, glial cells, including microglia and astrocytes, can be

240 activated by blood-serum proteins due to the disruption of the blood-brain barrier. Microglia
241 upregulate proinflammatory cytokines that leads to neurodegeneration. The activated
242 astrocytes and microglia encapsulate implanted devices by forming a dense scar tissue around
243 them. The astroglial reactivity increases the expression of connexin (CX43) that further promote
244 the inflammation in the nearby tissue. Reducing the electrode size and stiffness has shown to
245 reduce the immunoresponse by preventing the activation of astrocytes, reducing the
246 upregulation of inflammatory signaling (e.g. TNF α and IL-1 β) and avoiding injury to blood-brain-
247 barrier.

248

249 Electrochemical deposition at the cross-sectional surface of ultrathin substrates formed edge
250 electrodes⁶⁵. Not only can edge electrodes be made into small sizes, but they also increase the
251 volume of electrophysiologically-recorded tissue with electrophysiological access to neurons on
252 both sides of the thin-film substrates. It was demonstrated that gold electrodes with
253 electrochemically deposited PEDOT maintained stable electrochemical performance when
254 subjected to electrophysiological conditions (aqueous environment at 37 °C) for 60 days. The
255 PEDOT-based electrode array could be scaled to 1024 channels and record 375 single-unit
256 activity in freely behaving rats⁶⁶ (**Figure 4A**). Bodart et al. reported that a PEDOT-coated deep
257 brain stimulator (DBS) increased the charge storage capacity and operated *in vivo* for 2 weeks
258 with daily stimulation⁶⁷ (**Figure 4B**). EDOT-acid can improve the adhesion between metal and
259 conducting polymer and has the potential to further increase its aqueous stability⁶⁸. For chronic
260 implanted electronics such as DBS, the penetrating electrodes ideally should be stable in
261 physiological condition for more than 5 years, which remains a challenge for conjugated
262 polymer. Longer term *in vivo* evaluation of conjugated polymers is needed before translating
263 them into clinical applications.

264

265 The human brain is dynamic due to locomotion and cardiorespiratory cycles, and the micro-
266 motion leads to signal drift and instability in the brain-machine interface⁶⁹. Flexible electrodes
267 can potentially reduce the effects of micro-motion. The immunoresponse due to mechanical
268 mismatch between electrodes and electrogenic tissue also presents a great challenge for chronic
269 bio-interrogation⁷⁰. Glial response to stiff electrodes leads to insulating scar tissue formation
270 around electrodes³⁷. Reducing bending stiffness with structural design is one potential way to
271 reduce immunoresponse. Neurolink Co. developed a suture-like neural probe with high
272 bandwidth⁷¹. Bending stiffness mismatch between neural tissue and PEDOT coated electrodes
273 (**Figure 4C**) were reduced due to its ultrathin (~5 μ m) structure and low thread width (5-
274 50 μ m)⁷¹. Surface modification with PEDOT:PSS resulted in a lower impedance and higher
275 charge-carrying capacity when compared with IrOx modification (**Figure 4D**). 3000 electrodes on
276 the threads were inserted in a rat brain with the assistance of an advanced robotic system for
277 simultaneous recording (**Figure 4E**).

278

279 Another way to combat immunoresponse is to engineer the Young's modulus of the neural
280 interface. Despite the challenge in developing soft electronic materials and fabrication
281 processes, engineering the intrinsic properties of electronic materials allows more freedom in
282 the geometry and design of the electronics. Especially, handling a thin film or thread-like device
283 with 5 – 10 μ m thickness during surgical implantation is challenging for most neurosurgeons. A
284 slightly thicker (e.g. ~ 50 μ m) device with tissue-like Young's modulus offers better clinical
285 practicability. Coating electrodeposited PEDOT:PSS (Young's modulus: ~2.6 GPa) with ionically
286 conductive (not electrically conductive) alginate hydrogel (Young's modulus: ~ 30 kPa) can
287 reduce the mechanical mismatch⁷². While alginate hydrogels offer improved mechanical

288 compliance and biocompatibility, they also reduce the neural recording signal. In fact, the
289 average percentage of detectable unit drops linearly as the alginate hydrogel thickness
290 increases. To avoid the trade-off between signal quality and biomechanical compatibility, **the**
291 **design concept of promoting an interconnected conduction pathway or network inside a soft**
292 **matrix have been most effective. For example**, Feig and coworkers developed a dual conductive
293 (i.e. both ionic and electronic conductive) hydrogel. The interpenetrating network hydrogel had
294 a conductivity of 23 Sm^{-1} . Notably, the mechanically tunable Young's modulus allows
295 researchers to match with that of interfaced electrogenic tissue³⁵. **By using a ionic liquid to**
296 **induce aggregation of PEDOT**, Liu et al. further developed a PEDOT:PSS hydrogel with Young's
297 modulus in the range of kilopascal (comparable to that of neural tissue), while achieving a high
298 electrical conductivity of 4700 Sm^{-1} . Based on the unique anisotropic swelling-deswelling of the
299 pure PEDOT:PSS hydrogel, a hydrogel electrode array with a feature size of $20 \mu\text{m}$ was
300 fabricated³⁴. Zheng and co-workers combined geometry design and modulus engineering to
301 further improve the biocompatibility profile of implantable electronics. They developed a
302 PEDOT-PEG copolymer-based suture electrode (diameter of $\sim 100 \mu\text{m}$) with Young's modulus
303 below 1 MPa ⁷³. Taking together a high aspect ratio and relatively low Young's modulus, the
304 suture electrode showed excellent biocompatibility and had a desirable form factor to integrate
305 into the daily practice of clinicians.
306

307 **3. Peripheral nerve electronic interface**

308 ***Localized and low-voltage neuromodulation***

309 Extra-neural electrodes are less invasive compared to inter-fascicular or interfascicular
310 electrodes and therefore are often used clinically **for vagus nerve or sacral nerve stimulation**⁷⁴.
311 Electrode (array) cuffs typically wrap around tubular-shaped nerves to form a tight interface.
312 Although the substrate and encapsulation of cuff electrodes are made up of soft elastomers,
313 such as PDMS, their electrode materials, such as platinum or platinum-iridium, are usually
314 rigid⁷⁵. Qi et al. reported a conducting polymer polypyrrole (PPy) electrode that provided a
315 stretchable sciatic nerve interface using a pre-stretching strategy⁷⁶. The PPy nanowire sustained
316 over ten thousand stretch-release cycles without significantly compromising electrical
317 performance. The relatively large electrode size and lack of top encapsulation limited its
318 application for localized neuromodulation. Liu et al. overcame this challenge by developing a
319 lithographically micropatterned, fully encapsulated stretchable microelectrode using an
320 electrically conductive PEDOT:PSS hydrogel³⁴ (**Figure 5A**). In order to accommodate sciatic nerve
321 movement during stretching of the leg, both the electrode and interconnect were designed to
322 be soft (Young's modulus $\sim 20 \text{ kPa}$) and stretchable. Electrically conductive hydrogel was used for
323 both interconnects and electrodes. Different from metal interconnects, nanoporous polymer
324 interconnects made of conducting polymer further reduces the impedance when compared with
325 conducting polymer-coated metals⁷⁷ (**Figure 5B**), which can be modeled by a modified
326 transmission line equivalent circuit³⁴. Interconnect architecture, besides electrode dimension,
327 can be used to modulate electrode properties for designing clinical electrodes. Leveraging the
328 dual conductivity in both electrodes and interconnect, the hydrogel-based neural interface gave
329 30 times higher current injection density compared with platinum electrode of the same size. In
330 addition, an ultralow voltage of 50 mV was sufficient to elicit leg movement upon stimulation on
331 the sciatic nerve. Low-impedance polymeric electronics have the potential to be used for VNS to
332 treat drug-resistant epilepsy and to modulate inflammation reflex⁷⁸ and the brain-gut axis⁷⁹.

333 ***Regenerative nerve guidance conduit***

335 Abundant free volume in the conducting polymer matrix allows electrolyte to diffuse in. Their
336 mixed conductive nature and excellent biomechanical compatibility make conducting polymers
337 an ideal candidate for functional nerve scaffolds, where conducting polymers not only provide
338 an immediate microenvironment for cells, but also provide chronic electrical stimulation. PPy
339 nanofiber-based scaffolds provided a high Faraday current density for direct current
340 stimulation⁸⁰. Song et al. showed that electrical stimulation of human induced stem cell-derived
341 neural progenitor cells led to upregulation of neurotrophic factor expression, which is important
342 for synaptic remodeling and nerve regeneration⁸¹. Direct current stimulation using a PPy/PLCL
343 nerve conduit induced nerve growth and functional recovery on a sciatic nerve with large (15
344 mm) defect (**Figure 5C**)⁸². It had similar performance compared with autograft and was
345 significantly better than a non-stimulated conduit.
346

347 An ideal nerve guide should disintegrate and biodegrade after nerve regeneration.
348 Biodegradable polymers, such as poly(Llactic acid-co-ε-caprolactone)(PLCL)⁸² or poly(L-lactide)⁸³
349 were typically mixed with polypyrrole, followed by electrospinning into nanofibers. However,
350 the conducting polymer was not degraded in those cases. Imine bonds are conjugated linkages
351 that can be broken down in weakly acidic environments, and thus can be explored as a potential
352 method to develop biodegradable conjugated polymers⁸⁴. Alternatively, water-soluble
353 conducting polymers such as poly[ammonium- (3-thienyl)ethoxypropanesulfonate] (SPT)⁸⁵ can
354 be used to construct bio-erodible devices that break down into polymers with molecular weights
355 lower than the renal filtration threshold, i.e. 30 kDa. For more examples, readers can refer to
356 comprehensive reviews^{86,87} regarding nerve regeneration with conducting polymers.
357

358 ***Growth-adaptive conjugated polymer for pediatric electronic medicine***

359 Human growth has largely been overlooked for current bioelectronics development, partly
360 because of the lack of available electronic materials. Young children implanted with devices like
361 VNS suffer from severe tissue constraints and functional damage as they grow^{88,89}. Liu et al.
362 developed a system of growth-adaptive soft electronics named “morphing electronics” or
363 MorphE⁹⁰ (**Figure 5D**). A viscoplastic conductor made from PEDOT:PSS and glycerol could be
364 permanently deformed by the strain from tissue growth and thus maintained a seamless
365 interface throughout adolescent development. Morphing electronics caused minimal damage to
366 the rat nerve and allowed chronic electrical stimulation and monitoring for 2 months without
367 disruption of functional behavior (**Figure 5E**). In contrast, commercial cuff electrodes cause
368 permanent damage due to chronic compression (**Figure 5F**). Although the authors only
369 demonstrated the concept of MorphE in the peripheral nervous system, the general strategy of
370 developing viscoplastic electronics can be applied widely to other pediatric implantable devices.
371 Additional viscoplastic electronics materials, such as bio-responsive, dielectric, semiconducting
372 materials can be further added into the library of morphing electronics to enable multimodal
373 functionalities for pediatric electronic medicine. It is important to develop electronic medicine
374 that is sensitive to the biology of growing children, rather than treating children as adults with
375 smaller body size. The new research area in growth-adaptive implantable electronics can solve
376 this long-standing problem in the pediatric population and lead to next-generation pediatric
377 electronic medicine.
378

380 **4. Cardiac bio-electronic Interface** 381 ***Accommodating a constantly moving organ***

382 Electrical rotors and focal impulses are proposed to be the key drivers of atrial fibrillation.
383 Electrophysiological mapping of those irregular electrical activities and subsequent accurate
384 identification of their spatial location enables patient-specific ablation, offering high efficacy and
385 fast treatment⁹¹. Conventional basket electrodes have low spatial resolution in centimeter scale
386 and do not accommodate with heart beating. Seamless mechanical coupling on a beating heart
387 and high-spatial-resolution mapping are the two challenges that stretchable conducting
388 polymers are uniquely suited to address. Inorganic electrode arrays have demonstrated
389 electrophysiological mapping in an *ex vivo* experiment using a wavy structure design⁹².
390 Intrinsically stretchable devices using elastic conducting polymer, on the other hand, offer more
391 compact interconnect packing and therefore improve the electrode density. Cardiac activities
392 were recorded by an all-polymer electrode array⁵⁰ on an extracted embryonic mouse heart.
393 Although global ECG-like electrical signals were recorded, localized signals were not observed
394 due to the large electrode size of 0.5 mm. Taking advantage of lithographical micropatterning,
395 an intrinsically stretchable PEDOT:PSS microelectrode with electrode size of 80 μ m was
396 developed⁹³ (**Figure 6A&B**). The stretchable array was used for epicardial mapping (on atria) in
397 chronic atrial fibrillation porcine model *in vivo*. The thin-film stretchable device mechanically
398 coupled with the dynamically beating heart and gives stable electrophysiological recordings.
399 Compared with the state-of-the-art endocardial-mapping techniques, the epicardial mapping
400 with stretchable organic microelectrodes gave 2 times higher atrial-to-ventricular signal ratio
401 and >100 times higher spatial resolution. It is worth noting that electrical local heterogeneity in
402 chronic atrial fibrillation was identified thanks to its cellular-level spatial resolution.
403

404 **Passive conductive constructs to bypass impaired cardiac tissue**
405 Cardiac disease such as myocardium infarction or neuromuscular disorder causes cellular death
406 and fibrosis, which impair the normal conduction pathways between cardiomyocytes. The lack
407 of electrical communication between cardiomyocytes further leads to arrhythmia and
408 asynchronous contraction. A conductive polymer patch with high ionic mobility can provide a
409 low-impedance interface between cardiomyocytes and bypass insulating scar tissues⁹⁴. The ion
410 mobility within a conjugated polymer scaffold is higher than that in solution due to the
411 contribution of electro-osmosis in the conjugated polymer network¹⁸. Self-doped conductive
412 polymer (poly-3-amino-4- methoxybenzoic acid, PAMB) had 30 times higher conductivity
413 compared with gelatin-based Gelfoam (a commercial product)⁹⁵. As a result, the PAMB
414 epicardial patch significantly increased electrical impulse propagation and synchronous
415 cardiomyocyte contraction across the scar region. Mawad et al. improved the stability of
416 Polyaniline (PANI) by utilizing the strong chelation between the dopant phytic acid and chitosan
417 substrate⁹⁶. The PANI patch increased the conduction velocity on the infarcted heart in an *ex*
418 *vivo* experiment (**Figure 6C**). Polydopamine can be used as a wet adhesive for the conductive
419 polymer-based cardiac patch for improved stability on a dynamically moving heart⁹⁷. The
420 conductive polymer could also be made into an ink form for printing directly onto cardiac tissue.
421 By *in situ* polymerization of polypyrrole and dopamine in presence of Fe³⁺, the printable polymer
422 rapidly formed bonds on the wet epicardia surface. The cardiac patches promoted
423 reconstruction and revascularization of the infarct myocardium⁹⁸.
424
425

426 5. Biomolecular interface for chronic diseases

427
428 Implanted drug delivery platforms are a promising way to address biochemically-treatable
429 chronic disease, as the possibility for localized delivery can help mitigate off-target or large-dose

430 effects from systemic administration. Implanted platforms that have achieved clinical translation
431 so far rely on passive processes like diffusion to deliver drugs; however, researchers are
432 increasingly interested in leveraging conjugated polymers for active control of drug release,
433 enabling dosing schemes like pulsatile or closed-loop drug delivery. A comprehensive study of
434 recent advances in this space was published earlier this year⁹⁹. Unfortunately, there are still no
435 clinical studies of conjugated polymer-based implanted drug delivery platforms, in large part
436 because of barriers associated with regulatory approval of new functional materials. Indeed,
437 validation of most reported conjugated polymer-based drug delivery systems has been limited
438 to *in vitro* demonstrations of efficacy. In this section, we will specifically highlight works that
439 have also included *in vivo* validation, as they are furthest along the pathway to clinical
440 translation.

441 ***Encapsulation and release of charged small molecule drugs***

442 Conjugated polymers can entrap charged drug molecules via electrostatic interactions, with
443 subsequent release occurring either passively via diffusion or counter ion exchange, or in a
444 controlled manner by applying electrochemical potentials to modulate the redox state of the
445 conjugated polymers. Boehler and coworkers used this controlled approach to release
446 dexamethasone (Dex), a charged anti-inflammatory drug, from flexible neural microelectrodes
447 implanted in a rat hippocampus in order to test its ability to mitigate inflammation from the
448 electrode insertion process³² (**Figure 7A**). Iridium oxide (IrOx) microelectrodes were coated in
449 PEDOT via electropolymerization, with Dex incorporated into the conjugated polymer film as a
450 dopant during the polymerization step at 19 ng / probe. Dex was released on-demand from the
451 PEDOT coatings by applying a cyclic voltammetry (CV) scan in a three-electrode configuration.
452 320 stimulation sessions were performed over the course of twelve weeks. While it is unclear
453 whether the active delivery of Dex had a significant therapeutic impact, the study noted that CV
454 stimulations could be done in fully awake animals without evoking reaction or inflammation in
455 the histology. Notably, bare IrOx had the best performance compared to PEDOT-only,
456 PEDOT/PSS, and PEDOT/Dex-coated electrodes, which was attributed to residues from the
457 PEDOT electropolymerization process. This surprising finding underscores the importance of
458 accounting for the biocompatibility of different synthetic routes and potential impurities that
459 may be introduced through manufacturing when designing conjugated polymer-based systems.

460 While drug encapsulation in conjugated polymer films may be sufficient for shorter-term
461 delivery of highly potent drugs, larger doses or longer implantation times necessitate higher
462 drug loading. One way to increase loading is to encapsulate drugs in conjugated polymer
463 nanoparticles embedded within a hydrogel depot, though this potentially compromises on
464 spatial control of delivery. Ge and coworkers used PPy nanoparticles to encapsulate either
465 negatively or positively charged molecules, which could then be released with the application of
466 a weak DC electric field to induce reduction or oxidation of the PPy, respectively¹⁰⁰ (**Figure 7B**).
467 For *in vivo* applications, fluorescein-laden PPy particles were encapsulated at 1 wt% in a
468 thermoresponsive PLGA-PEG-PLGA injectable hydrogel and shown to be biocompatible in mice.
469 To test triggerable release, a voltage was applied between the particle injection site and a
470 separate injection site. As expected, fluorescence from released fluorescein molecules was only
471 observed after application of an electric field. While this is an exciting proof-of-concept and
472 subsequent reports from the same group have shown that it is feasible to use their PPy

473 nanoparticle platform to deliver therapies like anti-cancer drugs and insulin^{101–103}, *in vivo*
474 demonstrations of therapeutic effect with these drugs are still needed.

475 **Drug-selective membranes for neurotransmitter delivery**

476 To simultaneously enable high drug loading capacity and high spatial control, organic electronic
477 ion pumps (OEIP) that incorporate conjugated polymers as drug-selective membranes are
478 increasingly being explored. In this design, drugs can be electrophoretically pumped across the
479 conjugated polymer membrane from a separate reservoir, thereby decoupling loading capacity
480 from the thickness of the conjugated polymer film, and high spatial control can be obtained by
481 using microfabrication techniques to fabricate devices. Agneta Richter-Dahlfors and colleagues
482 used photolithographic patterning to fabricate planar ion pump devices with PEDOT:PSS (**Figure**
483 **7C**) to deliver glutamate (Glu) in a voltage-dependent manner to the auditory system of guinea
484 pigs¹⁰⁴ (**Figure 7D**). Glu is a neurotransmitter that is negatively charged at neutral pH and acts on
485 inner hair cells of the cochlea to transduce sound waves. Shifts in the auditory brain response
486 (ABR) threshold illustrated the effect of Glu in real time: after 60 minutes of continuous delivery,
487 a statistically significant shift in ABR threshold was observed at all tested frequencies. Notably,
488 excitotoxic swelling was observed in some inner cell dendrites, suggesting that better temporal
489 control of delivery is desirable for this application. For future investigations, their platform could
490 readily accomplish this by modulating the electrophoretic driving voltage with time, for instance
491 using pulsatile instead of continuous release.

492 In the first demonstration of an organic electronic delivery device implanted into an awake and
493 moving animal for therapeutic purposes, Johnsson et al. implanted a PEDOT:PSS-based OEIP
494 device into the spinal cord of a spared nerve injury (SNI) rat model to locally deliver GABA, the
495 primary inhibitory neurotransmitter in the central nervous system¹⁰⁵. Implantation did not lead
496 to any observable signs of spinal cord injury. Tactile hypersensitivity is a feature of the SNI
497 model, and is characterized by unusually low threshold of applied tactile force needed to induce
498 a brisk withdrawal of the hindlimb (withdrawal threshold, WT). Validating the therapeutic effect
499 of drug delivery from the device, rats that received GABA⁺ from implanted OEIPs showed
500 significant increases in WTs compared to those that received H⁺, which was used as the negative
501 control.

502 Recently, a modified OEIP called a microfluidic ion pump (μ FIP) was reported that simplifies the
503 process of replenishing the ion reservoir, allowing for high drug loading over even longer
504 implanted timescales^{106,107}. Proctor et al. fabricated neural probes consisting of μ FIPs to deliver
505 the neurotransmitter GABA to the hippocampus as a therapeutic agent for epilepsy¹⁰⁷. By
506 combining ^{106,107} μ FIPs with recording electrodes, the authors were able to detect seizure-like
507 events (SLEs) in mice induced by local injection of 4-aminopyridine (4AP), then immediately
508 trigger the local delivery of GABA, after which no additional SLEs were observed (**Figure 7E**). The
509 authors also demonstrated that GABA delivered prior to 4AP injection could prevent SLEs from
510 occurring, suggesting that predictive electrophysiological analysis could potentially be combined
511 with on-demand drug delivery to create closed loop epilepsy treatments (**Figure 7E**). Notably,
512 because only a small dose of GABA was needed to inhibit neural activity (local concentration of
513 10^{-5} M), each dose represented less than 1% of the device's total drug loading capacity,
514 indicating the potential for long-term delivery even without replenishment of the reservoir.

515 As conjugated polymers continue to be explored for drug delivery, it will be important to
516 carefully assess not just the biocompatibility of these materials, but also of the byproducts and
517 contaminants encountered during their syntheses. Additionally, the different on-demand drug
518 delivery architectures should be weighed based on application- and drug-specific requirements
519 regarding drug load, implantation timeframe, and the importance of spatial and temporal
520 control. It will also be important to consider what may happen in the case of premature device
521 failure. For instance, while reservoir-based delivery strategies like the μ FIP increase drug
522 loading, they also pose new clinical challenges in the case of reservoir failure, which could
523 expose surrounding tissues to a potentially toxic concentration of the drug⁹⁹. In light of the
524 regulatory barriers associated with conjugated polymers, sufficiently addressing potential safety
525 concerns is particularly crucial for successful clinical translation.

526

527 **6. Distributed interface for electrogenic tissue**

528 ***Spatially distributed implantable system***

529 Most electronic medicine relies on integrated and centralized biosignal acquisition and power
530 supply. Implanted power supplies such as batteries often contribute most of the volume in
531 implantable bioelectronic systems and thus prevent their miniaturization and interrogation
532 precision. Furthermore, the physical electronic interconnect for biosignal transmission occupies
533 substantial space, often more than the implantable electrodes or sensors themselves. A wireless
534 system without a physical (or materialized) interconnect between the biointerface and signal
535 processing unit could potentially reduce invasiveness and allow higher bandwidths. Ultrasound
536 can power a wireless neural interface for electrophysiological stimulation^{108,109}. Johnson et al.
537 developed StimDust, a peripheral nerve stimulator that received ultrasound input and converted
538 it into electrical stimulation with a piezocrystal¹¹⁰(**Figure 8A**). Individual Stimdust with a volume
539 of 6.5 mm³ has been demonstrated to activate the sciatic nerve of anesthetized rodents.
540 PEDOT:PSS was electroplated on Au electrode to further reduce the electrochemical impedance.
541

542 Electromagnetic energy coupling is another option for wireless communication. Khalifa et al.
543 reported an electromagnetically powered 2-coil wireless system, the smallest implantable free-
544 floating neural stimulator with a device (including integrated circuit, electrodes and coil) volume
545 of only 0.009 mm³. The device was small enough to be delivered by a surgical needle as an
546 injectable neurostimulator (**Figure 8B**). Inkjet-printed PEDOT:PSS/CNT electrodes at the cross-
547 sectional area of the silicon dies substantially reduced impedance and allowed effective
548 neuromodulation *in vivo*¹¹¹.

549

550 Near-infrared (NIR) radiation at 760 – 1500 nm wavelength can also be used to deliver energy to
551 implantable electronics thanks to its high penetration depth (4 - 10 cm)¹¹². Pyroelectric materials
552 like polyvinylidene difluoride (PVDF) can be sandwiched between two PEDOT:PSS electrodes to
553 construct a pyroelectric generator to power the neural interface. Upon NIR irradiation, the
554 device was able to electrically stimulate the gastrocnemius muscle of a frog. The high NIR
555 transmittance of PEDOT:PSS prevented high local temperature accumulation and allowed
556 stacking of multiple PEDOT:PSS/PVDF/PEDOT:PSS structures to increase output voltage¹¹³.

557

558 As a p-type conjugated polymer with good biocompatibility, poly(3-hexylthiophene) (P3HT) can
559 convert visible light into electrical stimulation for retinal prostheses¹¹⁴. Excitons generated from
560 P3HT upon illumination can be collected by an organic anode, PEDOT:PSS. Poly(3-

561 hexylthiophene)/ [6,6]-phenyl-C61-butyric acid methyl ester (P3HT/PCBM) blend can function as
562 an organic photovoltaic retinal interface. Ghezzi et al. demonstrated restoration of light
563 sensitivity in explants of blind rat retinas without PCBM by using just P3HT and PEDOT:PSS,
564 relying on the capacitive charging of the polymer–electrolyte interface rather than charge
565 transfer in conventional solar cells¹¹⁵. Excellent flexibility of the PEDOT:PSS and P3HT enabled a
566 foldable thin-film device structure that could be delivered via a small scleral incision and
567 conform to the curved eye surface^{116,117}. The organic photovoltaic prosthesis was capable of
568 wide-angle (visual angle of 46.3 degrees) and high-density (2215 stimulating pixels) stimulation
569 on retinal ganglion cell.. Maya-Vetencourt et al. demonstrated that the organic photovoltaic film
570 after implantation rescues light sensitivity and spatial acuity in retinitis pigmentosa for 6-10
571 months *in vivo*¹¹⁷(**Figure 8C**). This work showed the possibility of long-term neuronal
572 photostimulation with biocompatible conjugated polymer devices. The pixel density of the
573 flexible film-based retinal prosthesis was still an order of magnitude lower than the mosaic of
574 foveal cones (4-5 μ m) in healthy eyes, and therefore yields a poor spatial resolution. The same
575 research group recently reported a P3HT nanoparticle (~ 300 nm in size) system that can be
576 directly injected into subretinal space¹¹⁸(**Figure 8D**). The nanoparticle was tightly wrapped by
577 cell membrane extracellularly, forming a 20 nm cleft and therefore a high junction resistance for
578 effective localized stimulation. The photocurrent of capacitive origin triggered millivolt-level
579 depolarization on multiple sites on the cell membrane and elicited action potential when
580 membrane potential from temporospatial summation of cell-P3HT nanoparticle induced
581 potential surpassed the threshold. The liquid retinal prosthesis, as a non-genetic
582 photostimulator, allows a minimally invasive injection procedure and rescued sensitivity in a
583 blind rodent model with high spatial resolution and very prolonged effects. Although not
584 demonstrated in human clinical studies yet, distributed conjugated polymer-based devices have
585 the potential for treating patients with degenerative blindness without the need for the bulky
586 power supply and cameras used in conventional electrical stimulation systems.
587

588 ***In vivo synthesized bottom-up neural interface***

589 Implanting prefabricated electronics into biological tissue for a long time has been regarded as
590 the default neural interface configuration. *In situ* formation of neural interface, referred to here
591 as bottom-up neural interfacing, offers a different but exciting path towards seamless bio-
592 integration. Conjugated polymers have unique advantages for *in situ* synthesis or assembly in a
593 bio-environment at body temperature. One can leverage the polymerization of conjugated
594 polymers at defined spatial locations to construct neural interfaces in a bottom-up fashion. An
595 early attempt polymerized polypyrrole into a porcine pericardium. However, it used cytotoxic
596 chemical-initiated polymerization and failed to achieve electronic functionality¹¹⁹. In another
597 study, researchers chemically oxidize biocompatible 3,4-ethylenedioxylthiophene (EDOT)
598 monomers by Fe³⁺ *in situ* on acellular muscle tissue constructs, rather than living tissue¹²⁰.
599 Richardson-Burns et al. demonstrated the first direct polymerization of PEDOT in living neural
600 tissue¹²¹ (**Figure 8E**). In the electrochemical polymerization, nanoscale PEDOT filaments grew out
601 from a gold electrode and formed a cloud of conducting polymer deeply integrated with neural
602 tissues. The PEDOT filaments extending into the extracellular matrix substantially lowered the
603 electrochemical impedance for improved electrical communication between neurons and the
604 neurodevice. Beside, this PEDOT cloud with a few hundred microns to millimeter size could
605 penetrate electrically insulating glial scar tissue, which is around 0.1 -0.15 mm in thickness, and
606 thus has the potential to overcome the challenge of device failure due to foreign body
607 responses. *In vivo* polymerized PEDOT in rat cerebral cortex improved action potential signal
608 quality with lower recording noise and higher signal-to-noise ratio¹²².

609
610 Ouyang et al. further studied the long-term biocompatibility of the *in vivo* polymerized PEDOT as
611 a potential chronic neural implant¹²³. In this study, a microcannula delivered EDOT monomer
612 into the dorsal hippocampus for spatially-targeted electrochemical deposition. *In vivo*
613 polymerization of PEDOT did not impair the rat's ability to perform the hippocampus-dependent
614 behavioral task of delayed alternation (DA). Although polymerized PEDOT can reduce
615 electrochemical impedance by formation of electrical contact across the scar tissue in the brain,
616 secondary immunoresponse characterized by ED1 and GFAP biomarkers was observed after 2
617 weeks of polymerization. Further optimization of electrochemical polymerization parameters is
618 required to prevent secondary damage (during polymerization) to the interfaced tissue.
619
620 Current neuroelectronic interfaces lack genetic specificity and therefore are unable to
621 selectively interface with specific cellular types. Liu et al. developed a genetically targeted
622 chemical assembly method to introduce conducting polymers directly onto cell membranes¹²⁴
623 (**Figure 8F**). Humanized version of ascorbate peroxidase Apex2 was selectively expressed in a
624 specific neuronal type and was used to catalyze the polymerization of conducting polymer in the
625 presence of a low concentration of hydrogen peroxide. Polyaniline dimer, rather than monomer,
626 was used to reduce the oxidation potential, so that polymerization could occur at physiological
627 conditions. The polyaniline coated onto cell membranes increased membrane capacitance and
628 therefore reduced the action potential amplitude, which could be used to modulate cell
629 membrane properties. As an example, the authors reduced the pumping frequency of
630 pharyngeal muscle in *Caenorhabditis elegans* by using the inhibitory role of polyaniline coated
631 on the neurons. This new method of conducting polymer assembly has potential for clinical
632 application where genetic specificity is required. Further improvement is needed, including
633 minimizing chronic cytotoxicity in mammals and increasing electrical conductivity of the
634 synthesized polymer, as is addressing regulatory considerations surrounding genetic
635 modification of cells.
636
637
638 **Conclusion and outlook**
639 The repertoire of unique properties in conjugated polymers has substantially expanded over the
640 past decades and is continuously growing. Those unique properties address two of the most
641 important challenges in implantable electronic medicine. The two challenges faced by current
642 implantable bioelectronics are (1) electrical: how to efficiently facilitate ionic-mediated charge
643 transport at the tissue-electronic interface, and (2) mechanical: how to maintain seamless
644 electronic contact to living tissue and co-exist with minimal disturbance to normal biological
645 activity. Conjugated polymers, especially conducting polymers with mixed ionic and electronic
646 conductivity, contribute to low electrochemical impedance of electrodes, high transconductance
647 of electrochemical transistors, and high ion mobility of regenerative electrical patches.
648 Meanwhile, tissue-like mechanical properties, including softness, flexibility, and stretchability,
649 allow a stable and adaptive interface to couple with dynamically moving or rapidly growing
650 electrogenic tissue, and lay the foundation for chronic, mechanically transparent,
651 immunoresponse-free, and seamless bio-electronic integration. Additionally, the tunable redox
652 state of conjugated polymers allows for controlled release of pharmaceutical drugs by doping
653 and de-doping. Looking forward, development in this area will continue in the direction of
654 tissue-mimicking, personalized, and precision electronic medicine.
655

656 Conjugated polymer-based implantable electronics show promise in treating cardiac disease,
657 neurological disorders, and other chronic disease. Currently, PEDOT-based ECoG electrode
658 arrays for epilepsy have been tested on 30 human subjects and are furthest along the pipeline
659 of clinical translation⁵⁷. However, most other works have demonstrated potential so far only in
660 small animal models (e.g. rodents). To move beyond small animal models to big animal models,
661 clinical studies, and eventually clinical adoption, certain significant challenges will still need to
662 be overcome. Compared with existing inorganic bioelectronic interfaces, aqueous stability of
663 conducting polymers remains one of the biggest challenges to extend their lifetime. Some
664 implantable electronics such as Intracranial electroencephalography (iEEG) last a few weeks
665 inside the human body. Others such as vagus nerve stimulators expect to last more than 5
666 years. Yet, stability experiments (e.g. accelerated aging test) on conjugated polymers at such
667 time scales are rare. To overcome stability limitations, chemical strategies can be devised such
668 as direct crosslinking, double network formation, or self-doping to minimize disintegration of
669 the dopant. Through molecular engineering directly on the backbone and/or side chain of the
670 conjugated polymers, we can further improve the their electrical conductivity and even
671 introduce new functionality such as in vivo biodegradability that can prevent additional
672 surgeries for removing the implant after treatment is completed.
673

674 Reliable sterilization techniques for operative procedures are also required. It has been
675 established that autoclave⁵⁶, ethylene oxide¹¹⁷ and gamma-ray radiation¹²⁵ do not significantly
676 change the electronic performance of PEDOT:PSS and PPy, respectively, but suitable sterilization
677 methods for other conjugated polymers are still lacking. Reliable and scalable microfabrication
678 methods to pattern soft conjugated polymers also need to be developed. Photolithography-
679 compatible fabrication schemes are especially important to construct fully encapsulated, multi-
680 layered device structures and high spatial resolution devices for precise communication at the
681 bio-electronic interface. Lastly, acquiring FDA approval for commercialization requires extensive
682 evaluation of clinical safety and efficacy. Especially for novel materials such as conjugated
683 polymers stringent biocompatibility, in-body stability, and cytotoxicity testing are required to
684 minimize their risk to the patients.
685
686

701 **Conflict of Interest**

702 The authors declare no conflict of interest.
703

704 **Acknowledgements**

705 Z.B. acknowledges support from the National Science Foundation Future Manufacturing
706 Program (award no. 2037164). Y.L. thanks the financial support from Agency for Science,
707 Technology and Research (A*STAR) under its AME Programmatic Funding Scheme (Project
708 #A18A1b0045).
709

710 **Keywords**

711 Conjugated polymer, bioelectronics, clinical translation, implantable electronics.
712

713 **References**

714 1. Allied Market Research. Medical Implants Market - Growth, Global Share, Industry
715 Overview, Analysis, Trends Opportunities and Forecast 2014 - 2020. *Allied Market*

717 Research (2016). Available at: <https://www.alliedmarketresearch.com/medical-implants->
718 market.

719 2. Guimard, N. K., Gomez, N. & Schmidt, C. E. Conducting polymers in biomedical
720 engineering. *Progress in Polymer Science (Oxford)* **32**, 876–921 (2007).

721 3. Zhu, C., Liu, L., Yang, Q., Lv, F. & Wang, S. Water-soluble conjugated polymers for
722 imaging, diagnosis, and therapy. *Chemical Reviews* **112**, 4687–4735 (2012).

723 4. Lange, U., Roznyatovskaya, N. V. & Mirsky, V. M. Conducting polymers in chemical
724 sensors and arrays. *Analytica Chimica Acta* **614**, 1–26 (2008).

725 5. Pecher, J. & Mecking, S. Nanoparticles of conjugated polymers. *Chem. Rev.* **110**, 6260–
726 6279 (2010).

727 6. Guo, X., Baumgarten, M. & Müllen, K. Designing π -conjugated polymers for organic
728 electronics. *Progress in Polymer Science* **38**, 1832–1908 (2013).

729 7. Li, C., Bai, H. & Shi, G. Conducting polymer nanomaterials: Electrosynthesis and
730 applications. *Chem. Soc. Rev.* **38**, 2397–2409 (2009).

731 8. Malinauskas, A. Chemical deposition of conducting polymers. *Polymer (Guildf.)* **42**, 3957–
732 3972 (2001).

733 9. Nezakati, T., Seifalian, A., Tan, A. & Seifalian, A. M. Conductive Polymers: Opportunities
734 and Challenges in Biomedical Applications. *Chemical Reviews* **118**, 6766–6843 (2018).

735 10. Mihailetschi, V. D., Xie, H., De Boer, B., Koster, L. J. A. & Blom, P. W. M. Charge transport
736 and photocurrent generation in poly(3-hexylthiophene): Methanofullerene bulk-
737 heterojunction solar cells. *Adv. Funct. Mater.* **16**, 699–708 (2006).

738 11. Heywang, G. & Jonas, F. Poly(alkylenedioxythiophene)s - New, very stable conducting
739 polymers. *Adv. Mater.* **4**, 116–118 (1992).

740 12. Letheby, H. On the production of a blue substance by the electrolysis of sulphate of
741 aniline. *J. Chem. Soc.* **15**, 161–163 (1862).

742 13. McNeill, R., Siudak, R., Wardlaw, J. H. & Weiss, D. E. Electronic conduction in polymers. I.
743 The chemical structure of polypyrrole. *Aust. J. Chem.* **16**, 1056–1075 (1963).

744 14. Zeng, W. *et al.* Fiber-based wearable electronics: A review of materials, fabrication,
745 devices, and applications. *Advanced Materials* **26**, 5310–5336 (2014).

746 15. Ray, T. R. *et al.* Bio-integrated wearable systems: A comprehensive review. *Chemical
747 Reviews* **119**, 5461–5533 (2019).

748 16. Teymourian, H. *et al.* Wearable Electrochemical Sensors for the Monitoring and
749 Screening of Drugs. *ACS Sensors* **5**, 2679–2700 (2020).

750 17. Jaiswal, M. & Menon, R. Polymer electronic materials: A review of charge transport.
751 *Polymer International* **55**, 1371–1384 (2006).

752 18. Stavriniou, E. *et al.* Direct measurement of ion mobility in a conducting polymer. *Adv.
753 Mater.* **25**, 4488–4493 (2013).

754 19. Deslouis, C., El Moustafid, T., Musiani, M. M. & Tribollet, B. Mixed ionic-electronic
755 conduction of a conducting polymer film. Ac impedance study of polypyrrole.
756 *Electrochim. Acta* **41**, 1343–1349 (1996).

757 20. Yuk, H., Lu, B. & Zhao, X. Hydrogel bioelectronics. *Chemical Society Reviews* **48**, 1642–
758 1667 (2019).

759 21. Rivnay, J. *et al.* Structural control of mixed ionic and electronic transport in conducting
760 polymers. *Nat. Commun.* **7**, (2016).

761 22. Wang, S. & Urban, M. W. Self-healing polymers. *Nature Reviews Materials* **5**, 562–583
762 (2020).

763 23. Tran, H., Feig, V. R., Liu, K., Zheng, Y. & Bao, Z. Polymer Chemistries Underpinning
764 Materials for Skin-Inspired Electronics. *Macromolecules* **52**, 3965–3974 (2019).

765 24. Oh, J. Y. *et al.* Intrinsically stretchable and healable semiconducting polymer for organic
766 transistors. *Nature* **539**, 411–415 (2016).

767 25. Tran, H., Feig, V. R., Liu, K. & Bao, Z. Fully degradable and stretchable semiconducting
768 polymers for transient electronics. in 6 (2020). doi:10.1111/12.2567584

769 26. Kenry, K. & Liu, B. Recent Advances in Biodegradable Conducting Polymers and Their
770 Biomedical Applications. *Biomacromolecules* **19**, 1783–1803 (2018).

771 27. Lu, Y., Aimetti, A. A., Langer, R. & Gu, Z. Bioresponsive materials. *Nature Reviews
772 Materials* **2**, (2016).

773 28. Lee, J. Y. & Schmidt, C. E. Amine-functionalized polypyrrole: Inherently cell adhesive
774 conducting polymer. *J. Biomed. Mater. Res. - Part A* **103**, 2126–2132 (2015).

775 29. Oyman, G. *et al.* Peptide-modified conducting polymer as a biofunctional surface:
776 Monitoring of cell adhesion and proliferation. *RSC Adv.* **4**, 53411–53418 (2014).

777 30. Gelmi, A., Higgins, M. J. & Wallace, G. G. Physical surface and electromechanical
778 properties of doped polypyrrole biomaterials. *Biomaterials* **31**, 1974–1983 (2010).

779 31. Zhang, H., Molino, P. J., Wallace, G. G. & Higgins, M. J. Quantifying Molecular-Level Cell
780 Adhesion on Electroactive Conducting Polymers using Electrochemical-Single Cell Force
781 Spectroscopy. *Sci. Rep.* **5**, (2015).

782 32. Boehler, C. *et al.* Actively controlled release of Dexamethasone from neural
783 microelectrodes in a chronic in vivo study. *Biomaterials* **129**, 176–187 (2017).

784 33. Svirskis, D., Travas-Sejdic, J., Rodgers, A. & Garg, S. Electrochemically controlled drug
785 delivery based on intrinsically conducting polymers. *Journal of Controlled Release* **146**, 6–
786 15 (2010).

787 34. Liu, Y. *et al.* Soft and elastic hydrogel-based microelectronics for localized low-voltage
788 neuromodulation. *Nat. Biomed. Eng.* **3**, 58–68 (2019).

789 35. Feig, V. R., Tran, H., Lee, M. & Bao, Z. Mechanically tunable conductive interpenetrating
790 network hydrogels that mimic the elastic moduli of biological tissue. *Nat. Commun.* **9**,
791 (2018).

792 36. Moshayedi, P. *et al.* The relationship between glial cell mechanosensitivity and foreign
793 body reactions in the central nervous system. *Biomaterials* **35**, 3919–3925 (2014).

794 37. Salatino, J. W., Ludwig, K. A., Kozai, T. D. Y. & Purcell, E. K. Glial responses to implanted
795 electrodes in the brain. *Nat. Biomed. Eng.* **1**, 862–877 (2017).

796 38. Huse, M. Mechanical forces in the immune system. *Nature Reviews Immunology* **17**, 679–
797 690 (2017).

798 39. Hochberg, L. R. *et al.* Neuronal ensemble control of prosthetic devices by a human with
799 tetraplegia. *Nature* **442**, 164–171 (2006).

800 40. Mukamel, R. & Fried, I. Human intracranial recordings and cognitive neuroscience.
801 *Annual Review of Psychology* **63**, 511–537 (2012).

802 41. Flesher, S. N. *et al.* Intracortical microstimulation of human somatosensory cortex. *Sci.
803 Transl. Med.* **8**, (2016).

804 42. Anumanchipalli, G. K., Chartier, J. & Chang, E. F. Speech synthesis from neural decoding
805 of spoken sentences. *Nature* **568**, 493–498 (2019).

806 43. Kwan, P., Schachter, S. C. & Brodie, M. J. Drug-resistant epilepsy [5]. *New England Journal
807 of Medicine* **365**, 2239–2240 (2011).

808 44. Parvizi, J. & Kastner, S. Promises and limitations of human intracranial
809 electroencephalography. *Nature Neuroscience* **21**, 474–483 (2018).

810 45. Matsuo, T. *et al.* Intrasulcal electrocorticography in macaque monkeys with minimally
811 invasive neurosurgical protocols. *Front. Syst. Neurosci.* (2011).
812 doi:10.3389/fnsys.2011.00034

813 46. Schander, A. *et al.* A Flexible 202-Channel Epidural ECoG Array with PEDOT: PSS Coated
814 Electrodes for Chronic Recording of the Visual Cortex. *IEEE Sens. J.* **19**, 820–825 (2019).

815 47. Castagnola, E. *et al.* Pedot-cnt-coated low-impedance, ultra-flexible, and brain-
816 conformable micro-ECoG arrays. *IEEE Trans. Neural Syst. Rehabil. Eng.* **23**, 342–350
817 (2015).

818 48. Kim, D. H. *et al.* Dissolvable films of silk fibroin for ultrathin conformal bio-integrated
819 electronics. *Nat. Mater.* **9**, 1–7 (2010).

820 49. Lee, W. *et al.* Nonthrombogenic, stretchable, active multielectrode array for
821 electroanatomical mapping. *Sci. Adv.* **4**, (2018).

822 50. Blau, A. *et al.* Flexible, all-polymer microelectrode arrays for the capture of cardiac and
823 neuronal signals. *Biomaterials* **32**, 1778–1786 (2011).

824 51. Noe, K. *et al.* Long-term outcomes after nonlesional extratemporal lobe epilepsy surgery.
825 *JAMA Neurol.* **70**, 1003–1008 (2013).

826 52. Chang, E. F. Towards large-scale, human-based, mesoscopic neurotechnologies. *Neuron*
827 **86**, 68–78 (2015).

828 53. Abidian, M. R. & Martin, D. C. Multifunctional nanobiomaterials for neural interfaces.
829 *Adv. Funct. Mater.* **19**, 573–585 (2009).

830 54. Khodagholy, D. *et al.* NeuroGrid: Recording action potentials from the surface of the
831 brain. *Nat. Neurosci.* **18**, 310–315 (2015).

832 55. Khodagholy, D. *et al.* Highly conformable conducting polymer electrodes for in vivo
833 recordings. *Adv. Mater.* **23**, (2011).

834 56. Ganji, M. *et al.* Development and Translation of PEDOT:PSS Microelectrodes for
835 Intraoperative Monitoring. *Adv. Funct. Mater.* **28**, (2018).

836 57. Paulk, A. C. *et al.* Microscale physiological events on the human cortical surface detected
837 with PEDOT:PSS Electrodes. *bioRxiv* (2019). doi:10.1101/770743

838 58. Owens, R. M. & Malliaras, G. G. Organic electronics at the interface with biology. *MRS*
839 *Bull.* **35**, 449–456 (2010).

840 59. Paulsen, B. D., Tybrandt, K., Stavrinidou, E. & Rivnay, J. Organic mixed ionic–electronic
841 conductors. *Nature Materials* **19**, 13–26 (2020).

842 60. Khodagholy, D. *et al.* In vivo recordings of brain activity using organic transistors. *Nat.*
843 *Commun.* **4**, (2013).

844 61. Khodagholy, D. *et al.* High transconductance organic electrochemical transistors. *Nat.*
845 *Commun.* **4**, (2013).

846 62. Faria, G. C., Duong, D. T. & Salleo, A. On the transient response of organic
847 electrochemical transistors. *Org. Electron.* **45**, 215–221 (2017).

848 63. Cea, C. *et al.* Enhancement-mode ion-based transistor as a comprehensive interface and
849 real-time processing unit for in vivo electrophysiology. *Nat. Mater.* **19**, 679–686 (2020).

850 64. Lee, W. *et al.* Transparent, conformable, active multielectrode array using organic
851 electrochemical transistors. *Proc. Natl. Acad. Sci. U. S. A.* **114**, 10554–10559 (2017).

852 65. Seymour, J. P., Langhals, N. B., Anderson, D. J. & Kipke, D. R. Novel multi-sided,
853 microelectrode arrays for implantable neural applications. *Biomed. Microdevices* **13**,
854 441–451 (2011).

855 66. Chung, J. E. *et al.* High-Density, Long-Lasting, and Multi-region Electrophysiological
856 Recordings Using Polymer Electrode Arrays. *Neuron* **101**, 21-31.e5 (2019).

857 67. Bodart, C. *et al.* Electropolymerized Poly(3,4-ethylenedioxythiophene) (PEDOT) Coatings
858 for Implantable Deep-Brain-Stimulating Microelectrodes. *ACS Appl. Mater. Interfaces* **11**,
859 17226–17233 (2019).

860 68. Wei, B., Liu, J., Ouyang, L., Kuo, C. C. & Martin, D. C. Significant Enhancement of PEDOT

861 Thin Film Adhesion to Inorganic Solid Substrates with EDOT-Acid. *ACS Appl. Mater. Interfaces* **7**, 15388–15394 (2015).

862 69. Perge, J. A. *et al.* Intra-day signal instabilities affect decoding performance in an intracortical neural interface system. *J. Neural Eng.* **10**, (2013).

863 70. Szarowski, D. H. *et al.* Brain responses to micro-machined silicon devices. *Brain Res.* **983**, 23–35 (2003).

864 71. Musk, E. An integrated brain-machine interface platform with thousands of channels. *J. Med. Internet Res.* **21**, (2019).

865 72. Kim, D. H., Wiler, J. A., Anderson, D. J., Kipke, D. R. & Martin, D. C. Conducting polymers on hydrogel-coated neural electrode provide sensitive neural recordings in auditory cortex. *Acta Biomater.* **6**, 57–62 (2010).

866 73. Zheng, X. S. *et al.* Evaluation of a conducting elastomeric composite material for intramuscular electrode application. *Acta Biomater.* **103**, 81–91 (2020).

867 74. Hassler, C., Boretius, T. & Stieglitz, T. Polymers for neural implants. *Journal of Polymer Science, Part B: Polymer Physics* **49**, 18–33 (2011).

868 75. Russell, C., Roche, A. D. & Chakrabarty, S. Peripheral nerve bionic interface: a review of electrodes. *Int. J. Intell. Robot. Appl.* **3**, 11–18 (2019).

869 76. Qi, D. *et al.* Highly Stretchable, Compliant, Polymeric Microelectrode Arrays for In Vivo Electrophysiological Interfacing. *Adv. Mater.* **29**, (2017).

870 77. Ganji, M., Tanaka, A., Gilja, V., Halgren, E. & Dayeh, S. A. Scaling Effects on the Electrochemical Stimulation Performance of Au, Pt, and PEDOT:PSS Electrocorticography Arrays. *Adv. Funct. Mater.* **27**, (2017).

871 78. Pavlov, V. A. & Tracey, K. J. The vagus nerve and the inflammatory reflex - Linking immunity and metabolism. *Nature Reviews Endocrinology* **8**, 743–754 (2012).

872 79. Breit, S., Kupferberg, A., Rogler, G. & Hasler, G. Vagus nerve as modulator of the brain-gut axis in psychiatric and inflammatory disorders. *Frontiers in Psychiatry* **9**, (2018).

873 80. Lee, J. Y., Bashur, C. A., Goldstein, A. S. & Schmidt, C. E. Polypyrrole-coated electrospun PLGA nanofibers for neural tissue applications. *Biomaterials* **30**, 4325–4335 (2009).

874 81. Song, S. *et al.* Controlling properties of human neural progenitor cells using 2D and 3D conductive polymer scaffolds. *Sci. Rep.* **9**, (2019).

875 82. Song, J. *et al.* Polymerizing pyrrole coated poly (l-lactic acid-co-ε-caprolactone) (PLCL) conductive nanofibrous conduit combined with electric stimulation for long-range peripheral nerve regeneration. *Front. Mol. Neurosci.* **9**, (2016).

876 83. Shi, G., Rouabchia, M., Wang, Z., Dao, L. H. & Zhang, Z. A novel electrically conductive and biodegradable composite made of polypyrrole nanoparticles and polylactide. *Biomaterials* **25**, 2477–2488 (2004).

877 84. Lei, T. *et al.* Biocompatible and totally disintegrable semiconducting polymer for ultrathin and ultralightweight transient electronics. *Proc. Natl. Acad. Sci. U. S. A.* **114**, 5107–5112 (2017).

878 85. Mawad, D. *et al.* An erodible polythiophene-based composite for biomedical applications. *J. Mater. Chem.* **21**, 5555–5560 (2011).

879 86. Ning, C., Zhou, Z., Tan, G., Zhu, Y. & Mao, C. Electroactive polymers for tissue regeneration: Developments and perspectives. *Progress in Polymer Science* **81**, 144–162 (2018).

880 87. Petty, A. J., Keate, R. L., Jiang, B., Ameer, G. A. & Rivnay, J. Conducting Polymers for Tissue Regeneration in Vivo †. *Chem. Mater.* **32**, 4095–4115 (2020).

881 88. Samuels-Reid, J. H. & Cope, J. U. Medical devices and adolescents: Points to consider. *JAMA Pediatrics* **170**, 1035–1036 (2016).

909 89. Samdani, A. F. *et al.* Anterior vertebral body tethering for immature adolescent idiopathic
910 scoliosis: one-year results on the first 32 patients. *Eur. Spine J.* **24**, 1533–1539 (2015).

911 90. Liu, Y. *et al.* Morphing electronics enable neuromodulation in growing tissue. *Nat.*
912 *Biotechnol.* **38**, 1031–1036 (2020).

913 91. Narayan, S. M., Shivkumar, K., Krummen, D. E., Miller, J. M. & Rappel, W. J. Panoramic
914 electrophysiological mapping but not electrogram morphology identifies stable sources
915 for human atrial fibrillation: Stable atrial fibrillation rotors and focal sources relate poorly
916 to fractionated electrograms. *Circ. Arrhythmia Electrophysiol.* **6**, 58–67 (2013).

917 92. Xu, L. *et al.* 3D multifunctional integumentary membranes for spatiotemporal cardiac
918 measurements and stimulation across the entire epicardium. *Nat. Commun.* **5**, (2014).

919 93. Liu, J. *et al.* Intrinsically stretchable electrode array enabled in vivo electrophysiological
920 mapping of atrial fibrillation at cellular resolution. *Proc. Natl. Acad. Sci. U. S. A.* **117**,
921 14769–14778 (2020).

922 94. Burnstine-Townley, A., Eshel, Y. & Amdursky, N. Conductive Scaffolds for Cardiac and
923 Neuronal Tissue Engineering: Governing Factors and Mechanisms. *Adv. Funct. Mater.* **30**,
924 (2020).

925 95. Chen, S. *et al.* A conductive cell-delivery construct as a bioengineered patch that can
926 improve electrical propagation and synchronize cardiomyocyte contraction for heart
927 repair. *J. Control. Release* **320**, 73–82 (2020).

928 96. Mawad, D. *et al.* A Conducting polymer with enhanced electronic stability applied in
929 cardiac models. *Sci. Adv.* **2**, (2016).

930 97. Wang, L. *et al.* Mussel-Inspired Conductive Cryogel as Cardiac Tissue Patch to Repair
931 Myocardial Infarction by Migration of Conductive Nanoparticles. *Adv. Funct. Mater.* **26**,
932 4293–4305 (2016).

933 98. Liang, S. *et al.* Paintable and Rapidly Bondable Conductive Hydrogels as Therapeutic
934 Cardiac Patches. *Adv. Mater.* **30**, (2018).

935 99. Chapman, C. A. R., Cuttaz, E. A., Goding, J. A. & Green, R. A. Actively controlled local drug
936 delivery using conductive polymer-based devices. *Appl. Phys. Lett.* **116**, (2020).

937 100. Ge, J., Neofytou, E., Cahill, T. J., Beygui, R. E. & Zare, R. N. Drug release from electric-field-
938 responsive nanoparticles. *ACS Nano* **6**, 227–233 (2012).

939 101. Hosseini-Nassab, N., Samanta, D., Abdolazimi, Y., Annes, J. P. & Zare, R. N. Electrically
940 controlled release of insulin using polypyrrole nanoparticles. *Nanoscale* **9**, 143–149
941 (2017).

942 102. Samanta, D., Hosseini-Nassab, N., McCarty, A. D. & Zare, R. N. Ultra-low voltage triggered
943 release of an anti-cancer drug from polypyrrole nanoparticles. *Nanoscale* **10**, 9773–9779
944 (2018).

945 103. Puiggallí-Jou, A., Del Valle, L. J. & Alemán, C. Encapsulation and Storage of Therapeutic
946 Fibrin-Homing Peptides using Conducting Polymer Nanoparticles for Programmed
947 Release by Electrical Stimulation. *ACS Biomater. Sci. Eng.* **6**, 2135–2145 (2020).

948 104. Simon, D. T. *et al.* Organic electronics for precise delivery of neurotransmitters to
949 modulate mammalian sensory function. *Nat. Mater.* **8**, 742–746 (2009).

950 105. Jonsson, A. *et al.* Therapy using implanted organic bioelectronics. *Sci. Adv.* **1**, (2015).

951 106. Uguz, I. *et al.* A Microfluidic Ion Pump for In Vivo Drug Delivery. *Adv. Mater.* **29**, (2017).

952 107. Proctor, C. M. *et al.* Electrophoretic drug delivery for seizure control. *Sci. Adv.* **4**, (2018).

953 108. Seo, D. *et al.* Wireless Recording in the Peripheral Nervous System with Ultrasonic Neural
954 Dust. *Neuron* **91**, 529–539 (2016).

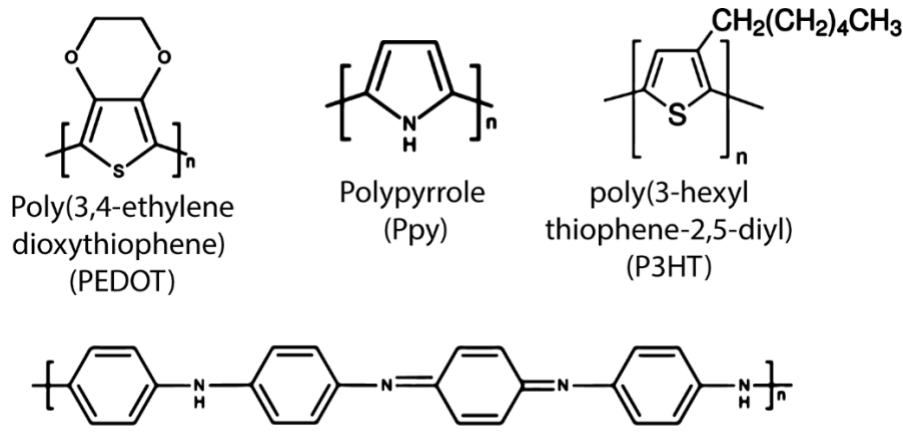
955 109. Seo, D., Carmena, J. M., Rabaey, J. M., Alon, E. & Maharbiz, M. M. Neural Dust: An
956 Ultrasonic, Low Power Solution for Chronic Brain-Machine Interfaces. (2013).

doi:arXiv:1307

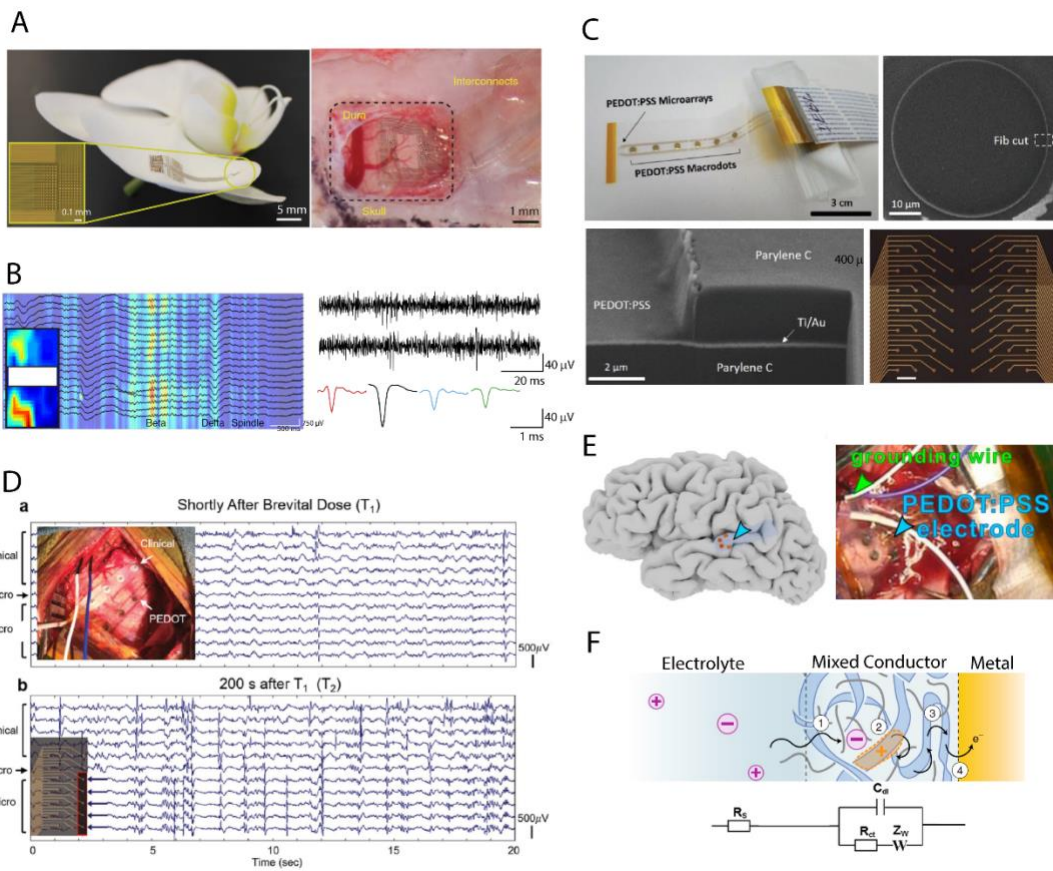
- 110. Johnson, B. C. *et al.* StimDust: A 6.5mm³, wireless ultrasonic peripheral nerve stimulator with 82% peak chip efficiency. in *2018 IEEE Custom Integrated Circuits Conference, CICC 2018* 1–4 (2018). doi:10.1109/CICC.2018.8357047
- 111. Khalifa, A. *et al.* The Microbead: A 0.009 mm³ Implantable Wireless Neural Stimulator. *IEEE Trans. Biomed. Circuits Syst.* **13**, 971–985 (2019).
- 112. Weissleder, R. A clearer vision for in vivo imaging: Progress continues in the development of smaller, more penetrable probes for biological imaging. *Nat. Biotechnol.* **19**, 316–317 (2001).
- 113. Jiang, W. *et al.* Laminated pyroelectric generator with spin coated transparent poly(3,4-ethylenedioxythiophene) polystyrene sulfonate (PEDOT:PSS) electrodes for a flexible self-powered stimulator. *RSC Adv.* **8**, 15134–15140 (2018).
- 114. Antognazza, M. R. *et al.* Characterization of a Polymer-Based, Fully Organic Prosthesis for Implantation into the Subretinal Space of the Rat. *Adv. Healthc. Mater.* **5**, 2271–2282 (2016).
- 115. Ghezzi, D. *et al.* A polymer optoelectronic interface restores light sensitivity in blind rat retinas. *Nat. Photonics* **7**, 400–406 (2013).
- 116. Ferlauto, L. *et al.* Design and validation of a foldable and photovoltaic wide-field epiretinal prosthesis. *Nat. Commun.* **9**, (2018).
- 117. Maya-Vetencourt, J. F. *et al.* A fully organic retinal prosthesis restores vision in a rat model of degenerative blindness. *Nat. Mater.* **16**, 681–689 (2017).
- 118. Maya-Vetencourt, J. F. *et al.* Subretinally injected semiconducting polymer nanoparticles rescue vision in a rat model of retinal dystrophy. *Nat. Nanotechnol.* **15**, 698–708 (2020).
- 119. Khor, E., Li, H. C. & Wee, A. In situ polymerization of pyrrole in animal tissue in the formation of hybrid biomaterials. *Biomaterials* **16**, 657–661 (1995).
- 120. Peramo, A. *et al.* In situ polymerization of a conductive polymer in acellular muscle tissue constructs. *Tissue Eng. - Part A* **14**, 423–432 (2008).
- 121. Richardson-Burns, S. M., Hendricks, J. L. & Martin, D. C. Electrochemical polymerization of conducting polymers in living neural tissue. *J. Neural Eng.* **4**, (2007).
- 122. Wilks, S. J., Woolley, A. J., Ouyang, L., Martin, D. C. & Otto, K. J. In vivo polymerization of poly(3,4-ethylenedioxythiophene) (PEDOT) in rodent cerebral cortex. in *Proceedings of the Annual International Conference of the IEEE Engineering in Medicine and Biology Society, EMBS* 5412–5415 (2011). doi:10.1109/IEMBS.2011.6091338
- 123. Ouyang, L., Shaw, C. L., Kuo, C. C., Griffin, A. L. & Martin, D. C. In vivo polymerization of poly(3,4-ethylenedioxythiophene) in the living rat hippocampus does not cause a significant loss of performance in a delayed alternation task. *J. Neural Eng.* **11**, (2014).
- 124. Liu, J. *et al.* Genetically targeted chemical assembly of functional materials in living cells, tissues, and animals. *Science (80-).* **367**, 1372–1376 (2020).
- 125. Kim, S. *et al.* Effective gamma-ray sterilization and characterization of conductive polypyrrole biomaterials. *Sci. Rep.* **8**, (2018).

1005
1006
1007
1008
1009
1010
1011
1012
1013
1014
1015
1016
1017
1018
1019
1020

Figures

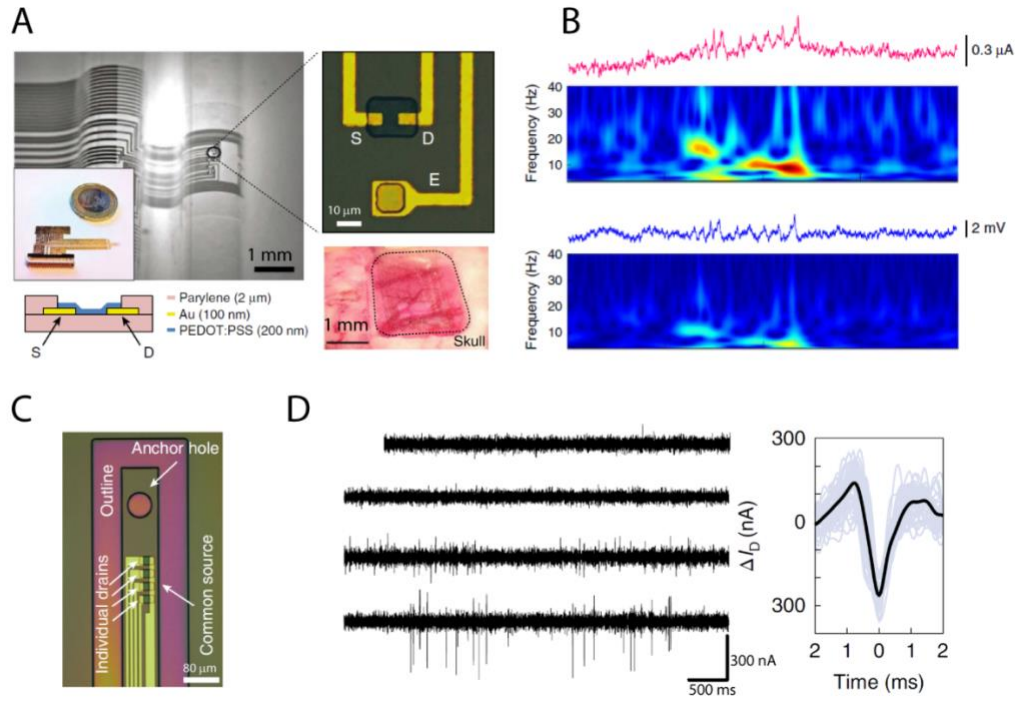


1021
1022 **Figure 1.** Chemical structures of common conductive polymers for bioelectronic applications:
1023 poly(3,4-ethylenedioxythiophene), polypyrrole, poly(3-hexylthiophene-2,5-diyl) and polyaniline.
1024
1025
1026
1027
1028
1029
1030
1031
1032
1033
1034
1035
1036
1037



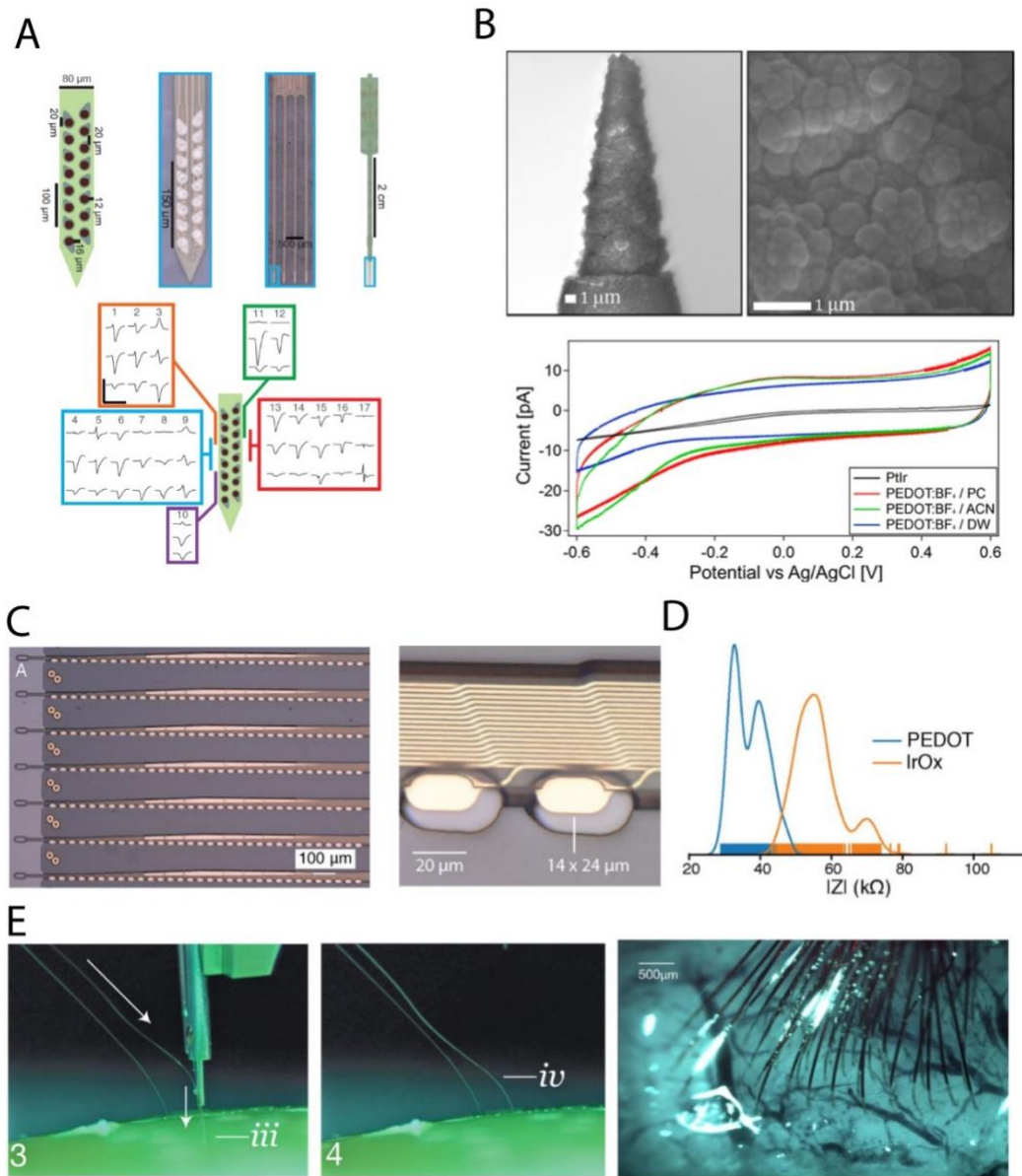
1038
1039
1040
1041
1042
1043
1044
1045
1046
1047
1048
1049
1050
1051
1052
1053
1054

Figure 2. Conducting polymer based ECoG Electrodes (A) PEDOT:PSS electrode array NeuroGrid conforms to a curved surface and rat somatosensory cortex. (B) Time-frequency spectrogram and Intraoperative recording of both local field potential (LFP) and spikes in epilepsy patients. Reproduced with permission.⁵⁴ Copyright 2015 Nature Publishing Group. (C) PEDOT:PSS electrophysiology device on thin-film parylene C layer with conformal and intimate contact between the different layers. (D) Simultaneously captured ECoG traces from clinical, PEDOT macro, and micro electrodes before and 200 s after epileptiform-inducing Methohexitol. Reproduced with permission.⁵⁶ Copyright 2018 Wiley. (E) PEDOT:PSS record on the surface of the human cortex. Reproduced under Creative Commons Attribution Licence.⁵⁷ (F) Charge transport in conjugated polymer as a ionic-electronic mixed conductor (1) dopant ion injection; (2) electronic carrier (hole) stabilization by a dopant ion (anion); (3) electronic carrier hopping (4) charge transfer between the metal electrode and the mixed conductor. The electrochemical impedance can be modelled by Randles circuit, where R_s , C_{dl} , R_{ct} and Z_w are electrolyte resistance, double layer capacitance, charge transport resistance and Warburg element. Reproduced with permission.⁵⁹ Copyright 2020 Nature Publishing Group.



1055
1056
1057
1058
1059
1060
1061
1062
1063
1064
1065
1066
1067
1068
1069
1070

Figure 3. Organic electrochemical transistor neural probes. **(A)** OECT EcoG probe conforms to curvilinear surface and somatosensory cortex. **(B)** The OECT recording and time-frequency analysis plot showed higher signal resolution for PEDOT:PSS based OECT (top) compared with an a PEDOT:PSS surface electrode (lower). Reproduced with permission.⁶⁰ Copyright 2013 Nature Publishing Group. **(C)** Optical micrograph of an e-IGT-based device with four transistors for LFP and spike recording. **(D)** High-pass filtered traces (250–2,500 Hz) from four e-IGTs in deep layers of rat cortex revealing waveforms suggestive of neural action potentials. Trigger averaging of waveforms demonstrated consistent action potential morphology. Reproduced with permission.⁶³ Copyright 2020 Nature Publishing Group.



1071
1072 **Figure 4.** Conducting polymer functionalized penetrating microelectrodes. (A) Electrochemically
1073 polymerized PEDOT electrode array. Stable and well isolated single-unit recording after 160 days
1074 of implantation. Reproduced with permission.⁶⁶ Copyright 2019 Elsevier (B) PEDOT:BF₄
1075 galvanostatically electropolymerized on PtIr electrode for deep brain stimulation. Cyclic
1076 voltammetry (CV) showed enhanced charge storage capacity for PEDOT-coated recording
1077 microelectrodes compared with uncoated ones. Reproduced with permission.⁶⁷ Copyright 2019
1078 American Chemical Society (C) Flexible thread-like electrode array with high density (32
1079 electrode contacts spaced by 50 μm) (D) Distribution of electrode impedances (measured at 1
1080 kHz) for two surface treatments: PEDOT (n=257) and IrOx (n=588). PEDOT coating yielded a
1081 lower electrode impedance compared with IrOx coating. (E) Implantation procedure for thread-
1082 like flexible electrode array. Multiple threads can be implanted at customized depth with
1083 assistance from automated needle penetration. Reproduced under Creative Commons
1084 Attribution License.⁷¹

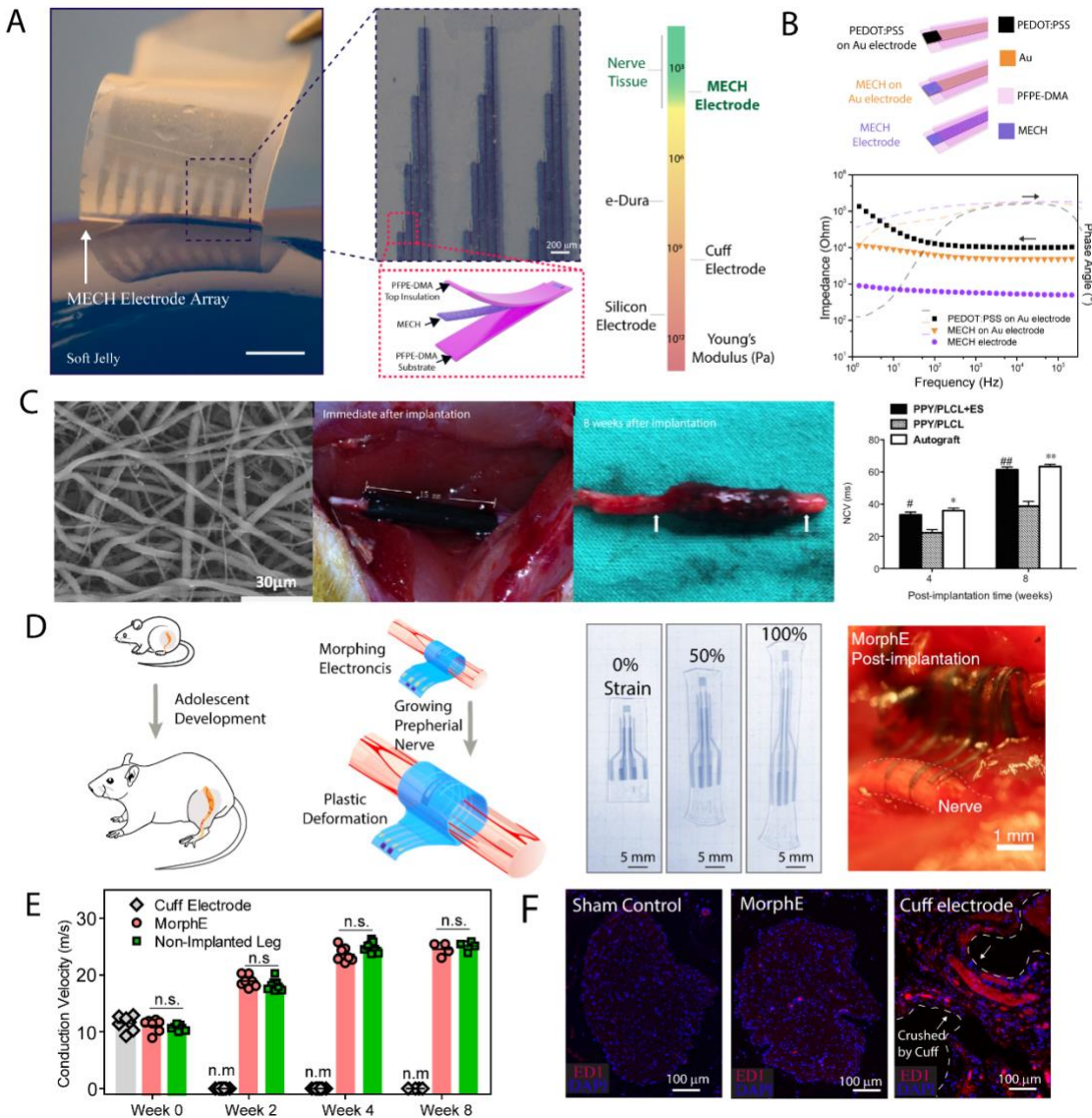
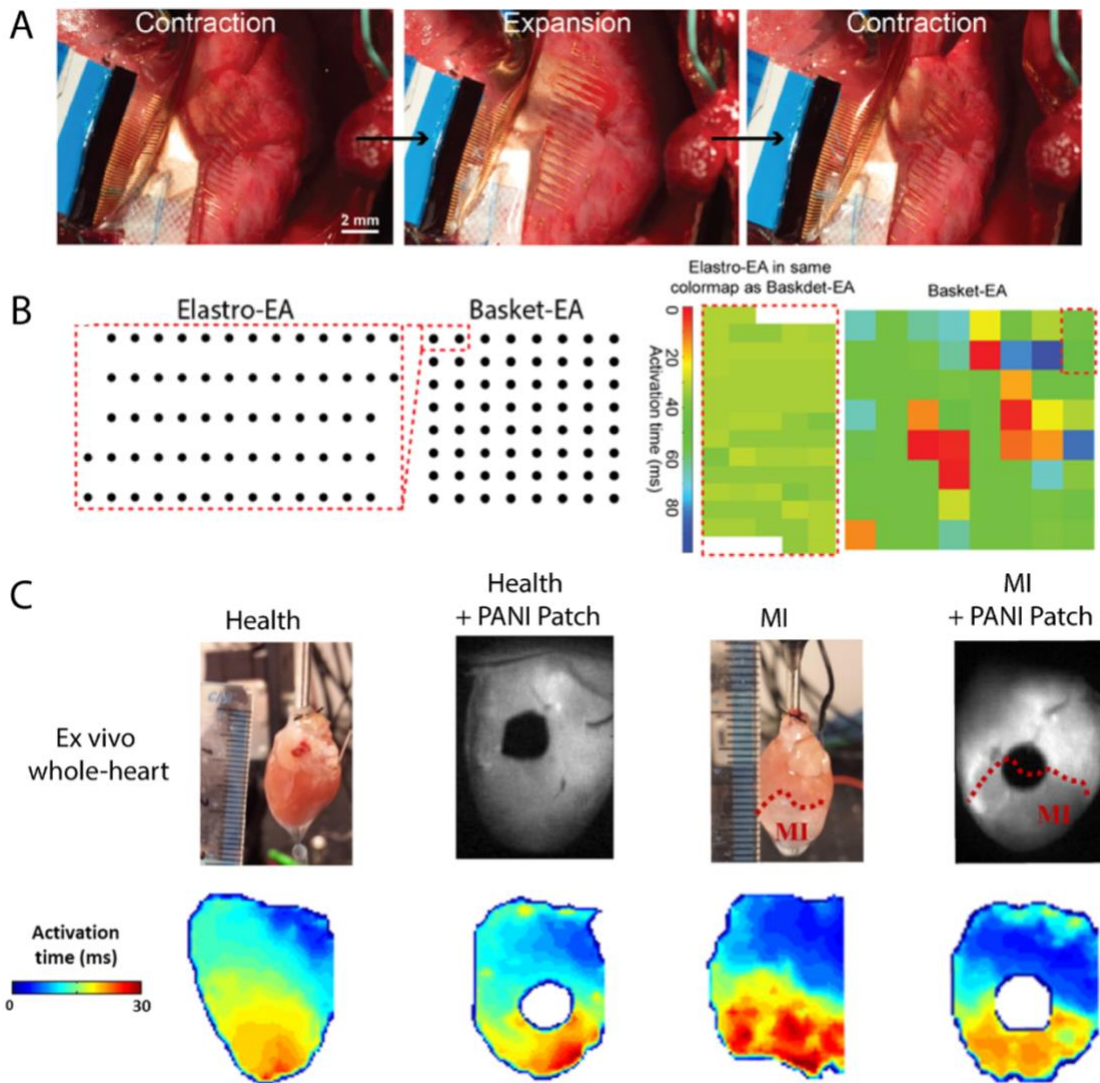


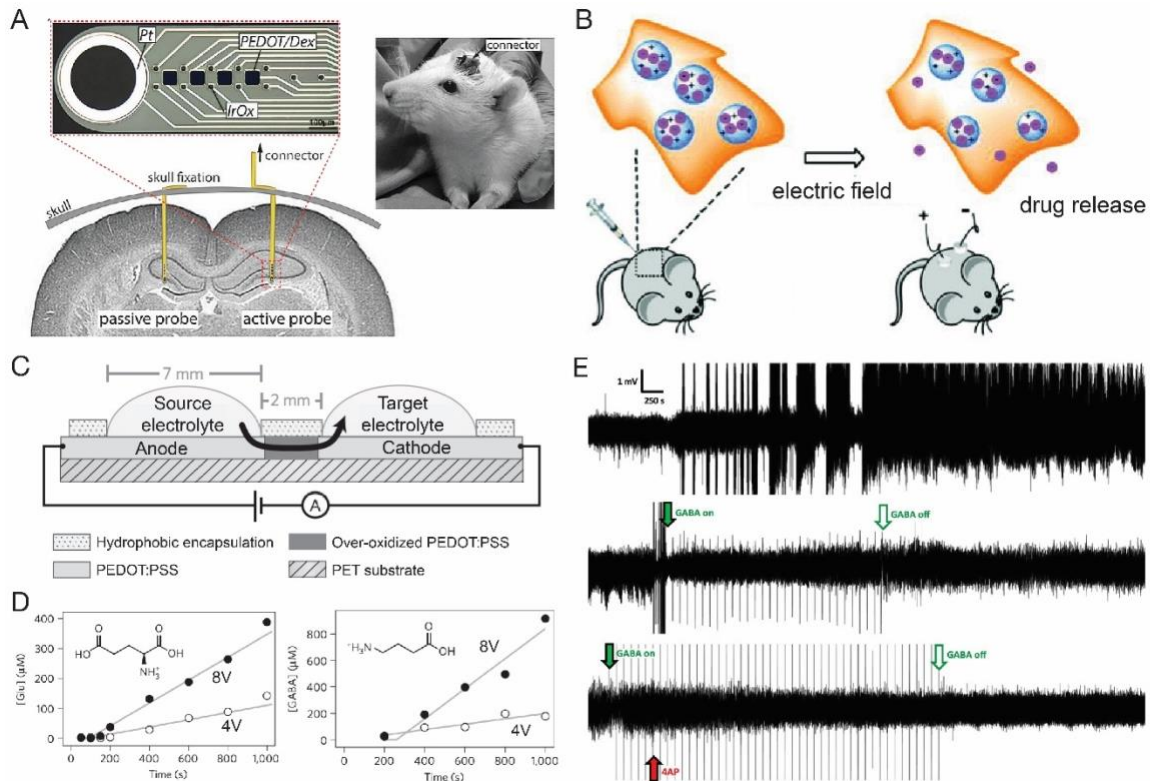
Figure 5. Soft peripheral neural interface. (A) Lithographically patterned hydrogel (MECH) elastronics with Young's modulus comparable to that of nerve tissue. (B) MECH electrodes (MECH as both interconnect and electrode) had substantially low electrochemical impedance compared with PEDOT:PSS or MECH coating on metal electrode. Reproduced with permission.³⁴ Copyright 2019 Nature Publishing Group. (C) 15 mm gaps of sciatic nerves were bridged using electrical stimulation of polypyrrole (PPy)/PLCL nanofibers based regenerative nerve conduit. Reproduced with permission.⁸² Copyright 2016 Frontiers Media S.A. (D) Morph electronics (MorphE), made of viscoplastic electronic materials, conformally adapts to sciatic nerve growth in vivo. (E) Rats implanted with MorphE had similar conduction velocities to nonimplanted nerve from week 0 to week 8 post-implantation, while cuff electrode failed after 2 weeks of implantation due to tissue outgrowth. (F) MorphE-implanted nerve had similar level of ED1 (a marker for inflammatory response) expression compared with sham control. Chronic compression resulted from non-adaptive cuff electrode led to high expression of ED1. Reproduced with permission.⁹⁰ Copyright 2020 Nature Publishing Group.

1085
1086

1087
1088
1089
1090
1091
1092
1093
1094
1095
1096
1097
1098
1099
1100

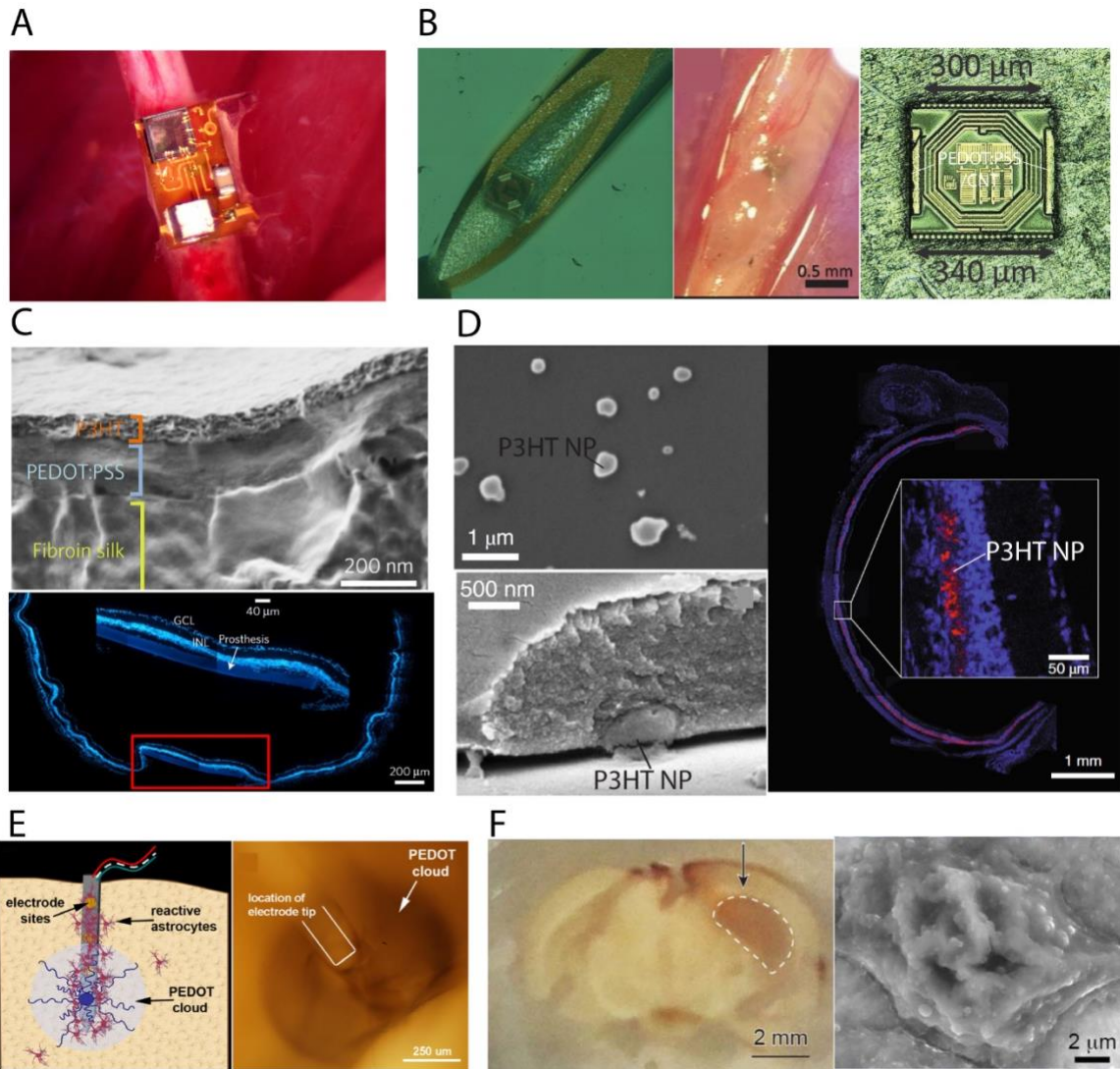


1101
1102 **Figure 6.** Active and passive cardiac interface with conducting polymer. **(A)** Intrinsically
1103 stretchable electrode array effectively prevented sliding and delamination from the epicardial
1104 surface during expansion/contraction of the right atrium in porcine with chronic atrial
1105 fibrillation. **(B)** Isochronal maps of activation time from endocardial basket electrodes and the
1106 epicardial elastrode array from the same temporal reference and scale. High-density elastrode
1107 detected localized electrical heterogeneity within the 10- to 30-ms time scale that can not be
1108 resolved using conventional clinical electrode array. Reproduced with permission.⁹³ Copyright
1109 2020 PNAS. **(C)** Representative activation time before and after PANI/Chitosan conductive patch
1110 application on healthy control hearts and on hearts 2 weeks after MI. The electrically conductive
1111 patch increased conduction velocity in the apical infarcted area. Reproduced with permission.⁹⁶
1112 Copyright 2016 AAAS.
1113
1114
1115
1116
1117
1118
1119



1120
1121 **Figure 7.** Conducting polymer-based devices for active drug delivery. **(A)** Flexible neural
1122 microelectrodes comprising PEDOT:PSS doped with the anti-inflammatory drug Dexamethasone,
1123 which was released on-demand after implantation into a rat hippocampus. Reproduced with
1124 permission.³² Copyright 2016 Elsevier. **(B)** PPy nanoparticles loaded into an injectable hydrogel
1125 can encapsulate charged small molecule drugs with high loading, with release triggered by
1126 application of an electric field. Reproduced with permission.¹⁰⁰ Copyright 2012 American
1127 Chemical Society. **(C)** Side view of an organic electronic ion pump (OEIP) with over-oxidized
1128 PEDOT:PSS as the drug-selective membrane. **(D)** The OEIP enables voltage-dependent delivery of
1129 neurotransmitters Glu and GABA. Reproduced with permission.¹⁰⁴ Copyright 2009 Nature
1130 Publishing Group. **(E)** Electrophysiology recordings showing seizure-like events (SLEs) (top),
1131 microfluidic ion pump delivery of GABA following SLE showing successful treatment (middle),
1132 and delivery of GABA to prevent SLE occurrence before prior to injection of 4AP. Reproduced
1133 with permission.¹⁰⁷ Copyright 2018 AAAS.

1134
1135
1136
1137
1138
1139
1140
1141
1142
1143



1144
1145 **Figure 8.** Conjugate polymer as distributed biointerface. (A) wireless ultrasonic peripheral nerve
1146 stimulator. Reproduced with permission.¹¹⁰ Copyright 2018 IEEE. (B) Electromagnetically
1147 powered 0.009 mm³ implantable wireless neural stimulator that can be delivered using surgical
1148 needles. Reproduced with permission.¹¹¹ Copyright 2019 IEEE. (C) Photovoltaic prostheses
1149 based on P3HT and PEDOT. The subretinal implants led to recovery of light sensitivity and visual
1150 acuity that persisted up to 6–10 months after surgery. Reproduced with permission.¹¹⁷ Copyright
1151 2017 Nature Publishing Group. (D) Conjugated polymer nanoparticles (P3HT NPs) mediate light-
1152 evoked stimulation of retinal neurons and persistently rescue visual functions when subretinally
1153 injected in a rat model of retinitis pigmentosa. Reproduced with permission.¹¹⁸ Copyright 2020
1154 Nature Publishing Group. (E) Polymerizing PEDOT directly into brain tissue from a neural
1155 electrode bypassed the surrounding glial scar to reduce the electrochemical impedance.
1156 Reproduced with permission.¹²¹ Copyright 2007 Institute of Physics Publishing. (F) Genetically
1157 instructing specific living neurons to guide chemical synthesis of PNAI at the cell membrane.
1158 Reproduced with permission.¹²⁴ Copyright 2020 AAAS.
1159